

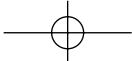




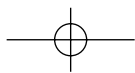
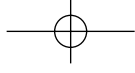
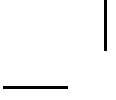


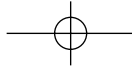
**Part One**  
**Cold Atoms and Molecules**



*Cold Atoms and Molecules*. Edited by Matthias Weidemüller and Claus Zimmermann  
Copyright © 2009 WILEY-VCH Verlag GmbH & Co. KGaA, Weinheim  
ISBN: 978-3-527-40750-7







# 1

## Cooling and Trapping of Atoms

*Peter van der Straten and Harold Metcalf*

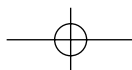
### 1.1

#### Introduction

The idea to use laser radiation to cool and trap atoms was first suggested by Wineland and Dehmelt [1] and independently by Hansch and Schawlow [2]. Since photons carry momentum, the momentum exchange between the laser radiation and the atoms in an absorption process can be used to apply a force on the atoms. Since the absorption depends on the difference between frequency of the laser radiation and the absorption frequency of the atoms, the absorption process can be made velocity-selective due to the Doppler effect, which shifts the atoms absorption frequency depending on its velocity. It is this simple notion that forms the basis for the research that has been carried out in the last 20 years in the field of laser cooling and trapping. Especially the velocity dependence of the process, leading to the fact that the forces are no longer conservative but can instead dissipate kinetic energy of the atoms, allows the experimentalists to cool atoms down to extremely low temperatures.

The initial ideas came about, since in atomic spectroscopy the resolution is limited by the Doppler effect, which shifts the absorption frequency. Since a thermal gas of atoms has a distribution of velocities, the Doppler shift leads to broadening of the absorption frequency. Already in the 1960s careful tricks have been designed to overcome this problem, but they always lead to smaller signals and therefore they ultimately limit the signal-to-noise in these experiments. Being able to cool the velocity distribution of the atoms and thus reduce its width without changing the number of atoms, is therefore very beneficial in those experiments.

Since the early experiments have been very successful in reducing the temperature of a cloud of atoms by many orders of magnitude, it became clear that laser cooling and trapping could be used in many more experiments and this opened a whole new field, which is nowadays known as laser cooling and trapping. For instance, since the temperature of the atoms is very low, the interaction energy becomes very small and thus interactions between the atoms can be studied in a whole new regime, the ultracold collision regime. Since the interaction time



#### 4 | 1 Cooling and Trapping of Atoms

between the atoms in this regime is much larger than the lifetime of the atoms in an excited state, absorption processes have to take place during the collision and thus the collisional system is probed during its interaction.

Furthermore, the energies of the atoms are becoming so small that atoms can be trapped in optical potentials, which have dimensions comparable to the wavelength of the light. This trapping of atoms in such small potentials with a periodicity given by the light field, the so-called optical lattice, is very reminiscent of the periodic potential an electron experiences in a crystal. Thus the physics to be studied in these optical lattices sheds light on the similarities and differences of phenomena, which take place at a very different length scale.

One of the most intriguing aspects of laser cooling and trapping is its ability to cool down a sample of atoms without losing any particles. Thus it became possible to increase the phase-space density of the atoms. Already from the onset of laser cooling and trapping it became clear that it could be instrumental in achieving a new phase of matter, the so-called Bose–Einstein condensed (BEC) phase. This phase had been predicted by Einstein on some original ideas by Bose in the 1920s, but its observation had always been hampered by the fact that it required a high density of atoms at very small temperatures. Compressing the atoms leads to an increase of the density, but at the same time increasing their temperature, yielding their phase-space density to remain constant. Adiabatic expanding the atoms volume leads to lowering of their temperature, but to a decrease of the density as well. However, using laser cooling techniques the temperature of the atoms can be lowered *without* changing the density, and thus it leads to an increase in the phase-space density.

In this chapter, we will not describe all the different schemes and techniques of laser cooling and trapping. Many of them can be found for instance in the *Laser Cooling and Trapping* book [3], which we recently published about the subject. Instead, we will focus on one aspect of it, namely on the techniques that have been used in the quest for BEC. In the beginning of the 1990s different experimental groups started to use laser cooling and trapping techniques to obtain the Bose condensed phase for the alkali-metal atoms. Although the actual quest for BEC took only 5 years, the ideas and techniques used originated back to all the work of the preceding 20 years. Not only did they rely on the results of laser cooling and trapping, in which the alkalis have been the prime atom to investigate due to its simple internal structure, it also relied on the work that took place to Bose condense atomic hydrogen, which had been carried out in parallel during the same period.

In the quest for BEC there have been many groups active and three American groups published the first results at about the same time (1995). These groups are listed in Table 1.1. They all used a different alkali with different atomic properties that are important for the achievement of BEC. The laser cooling techniques they used are different, but they all provided the low temperatures necessary for BEC. They all employed in the last phase of the cooling process the evaporation of atoms, which will be explained in detail at the end of this chapter. In this last phase the atoms were no longer held in an optical trap, since in the experiments

**Table 1.1** Summary of the achieved results of the three groups that published the first results on BEC for alkali-metal atoms in the year 1995.<sup>a</sup>

	JILA	Rice	MIT
Group	Cornell/Wieman	Hulet	Ketterle
Place	Colorado	Houston	Boston
Atom	<sup>87</sup> Rb	<sup>7</sup> Li	<sup>23</sup> Na
Nuclear spin $I$	$3/2$	$3/2$	$3/2$
Scattering length $a(a_0)$	+110	-30	+60
Cooling	Vapor cell MOT	Doppler slowing	Zeeman slowing
Trap	TOP	Permanent magnetic trap	Magnetic trap with optical plug
First BEC	June '95 [4]	July '95 [5]	September '95 [6]
$N_C$	$2 \times 10^4$	$2 \times 10^5$	$2 \times 10^6$
$T_C$ ( $\mu$ K)	0.1	0.4	2
$n_C$ ( $\text{cm}^{-3}$ )	$2 \times 10^{12}$	$2 \times 10^{12}$	$1.5 \times 10^{14}$
$\tau$ (s)	15	20	1

<sup>a</sup>In the table, we list the number of atoms in the condensate  $N_C$ , the temperature  $T_C$  at which the phase transition took place, and the density  $n_C$  of the atoms. Finally, the lifetime  $\tau$  of the condensate is shown.

it was discovered that in the final phase the use of light inhibited the further cooling and compression of the atoms. The numbers for the number of particles, the temperature, and the density given in the table are indicative for many other experiments in this field.

The chapter is designed as follows. After we discuss in Section 1.2 the general considerations regarding phase-space density, we will discuss in Section 1.3 the simplest model of laser cooling, the Doppler cooling. In Section 1.4, we will show, how laser light can be used to slow down a beam of atoms. Next in Section 1.5, we will show how laser light can be used to cool atoms in the so-called optical molasses. For the trapping of atoms in an optical trap many different schemes have been proposed, but in Section 1.6 we will only discuss the most popular version, the magneto-optical trap (MOT). In the experiments carried out at the end of the 1980s it became clear that the limit for laser cooling was not given by the result of the Doppler theory, as discussed in Section 1.3, but that atoms can be cooled to much lower temperatures. This work, nowadays referred to as sub-Doppler cooling, is described in Section 1.7. To trap atoms without laser light magnetic traps have been designed and implemented and we will describe them in Section 1.8. In Section 1.9, we will describe in a simple model the cooling technique that is most commonly used in the last phase of the cooling process, the evaporation of the atoms. In the last section, Section 1.10, we will describe the latest attempts to achieve BEC purely with optical techniques, before drawing some conclusions.

## 1.2

## Phase-Space Density

The phase-space density  $\rho(\vec{r}, \vec{p}, t)$  can be defined in terms of the probability that a single particle is at position  $\vec{r}$  and has momentum  $\vec{p}$  at time  $t$ . In classical mechanics it is possible to know position and momentum of a single particle with certainty simultaneously. In that case the phase-space density for a system of  $N$  particles is the sum of the phase-space densities of the single-particle phase-space densities of all the particles in the system divided by  $N$ . Since the phase-space density is a probability, it is always positive and can be normalized over the six-dimensional volume spanned by position  $\vec{r}$  and momentum  $\vec{p}$ .

For a gas of cold atoms it is convenient to define the phase-space density  $\rho$  as a dimensionless quantity

$$\rho = n\lambda_{\text{deB}}^3, \quad (1.1)$$

with  $\lambda_{\text{deB}}$  the deBroglie wavelength of the atoms in the sample as determined by their average velocity  $\bar{v}$ :

$$\lambda_{\text{deB}} = \frac{h}{M\bar{v}} = \frac{h}{\sqrt{3Mk_B T}}. \quad (1.2)$$

Note that the phase-space density can be increased by either increasing the density or by decreasing the average velocity  $\bar{v}$  of the atoms in the sample. For a thermal beam of atoms at room temperature at typical densities of  $10^{10}$  atoms/cm<sup>3</sup>, the phase-space density is of the order of  $10^{-17}$  (see Table 1.2). It can be shown that for a homogeneous gas of noninteracting atoms the transition from gas phase to the Bose–Einstein condensed phase occurs exactly at  $\rho = 2.612$  [7]. It is the object of laser cooling to increase the phase-space density over these many orders of magnitude.

In order to guide the discussion about the phase-space density and the road to BEC, Table 1.2 shows typical numbers of the phase-space density in different stages of laser cooling. Starting from the distribution of atoms in the oven, the

**Table 1.2** Typical numbers for the phase-space density as obtained in the experiments aimed at achieving BEC.<sup>a</sup>

Stages	$T$	$\lambda_{\text{deB}}$	$n$ (/cm <sup>3</sup> )	$n\lambda_{\text{deB}}^3$
Oven	300 °C	0.02 nm	$10^{10}$	$10^{-17}$
Slowing	30 mK	2 nm	$10^8$	$10^{-12}$
Cooling	1 mK	10 nm	$10^9$	$10^{-9}$
Trapping	1 mK	10 nm	$10^{12}$	$10^{-6}$
Evaporation	70 nK	1 μm	$10^{12}$	2.612

<sup>a</sup>The different stages of cooling and trapping the atoms will be explained in more detail in this chapter.

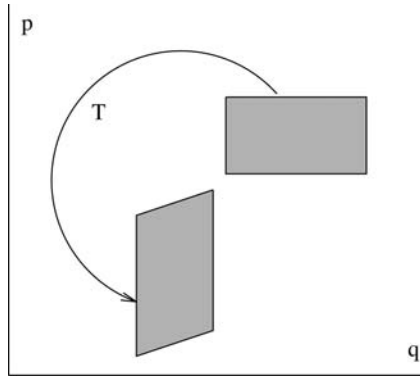


**Figure 1.1** By applying a conservative force the surface of phase space can be transformed into different shapes, but the total surface area is conserved.

effusive beam of atoms is slowed down from the thermal velocity down to tens of meters per second by slowing the atoms with laser light. Subsequently the atoms are cooled down by molasses cooling and trapped. Phase-space densities are of the order of  $10^{-6}$ , which is still six orders of magnitude away from the transition point. In the last step, evaporative cooling is used to increase the phase-space density to more than unity.

One important aspect to realize, is that the phase-space density cannot be changed by using conservative forces. In Figure 1.1, a schematic diagram is shown of a phase-space volume with spatial coordinates  $q$  and momentum coordinates  $p$ . If we now apply a transformation  $T$  in phase space, we can deform the volume and change its shape. However, the total volume in phase space remains constant and this is a result of the Liouville's theorem. For instance, in light optics one can focus a parallel beam of light with a lens to one point. In that case one has exchanged the high phase-space density due to the parallelism of the beam to a high density of light rays in the focus. However, the light rays in the focus are divergent. For classical particles the same principle applies. By increasing the strength of the trapping potential of particles in a trap, one can increase the density of the atoms in the trap, but at the same time the temperature of the sample increases leaving the phase-space density unchanged.

In order to increase the phase-space density, one has to apply a force on the atoms, which is no longer conservative. This can be achieved by having a force, which is dependent on the velocity or momentum of the atoms. In laser cooling we will see that the force on the atoms under certain conditions becomes a damping force, i.e., always directed opposite to the atomic velocity. In that case the phase-space density in momentum space increases. This process is irreversible caused by the spontaneous emission of the photons.

Laser cooling changes the temperature of the atoms. In thermodynamics we can only speak of a temperature, if the sample of atoms is in equilibrium with its surroundings. In laser cooling, this is usually not the case and in many

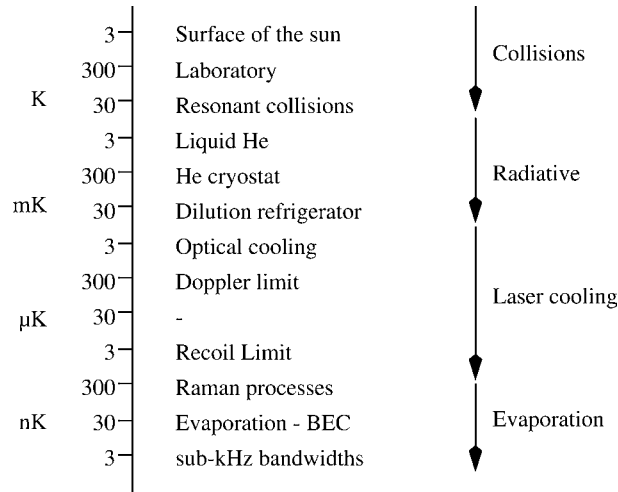


Figure 1.2 Temperature scale.

cases the atoms having temperatures far below 1 mK are trapped close to the walls of the vacuum chamber, which is at room temperature. However, for a Maxwell–Boltzmann distribution the spread of velocities is a direct measure of the temperature and we will use this fact to assign a temperature to a cooled sample of atoms, although the atoms are not in equilibrium. Typical temperatures involved in laser cooling are shown in Figure 1.2. As one can see laser cooling can cool down atoms from room temperature to below 1  $\mu$ m. The lowest temperatures are obtained by further cooling down the atoms by using evaporative cooling.

In order to show in more detail, how laser cooling can be used to increase phase-space density, we consider the cooling and collimation of an atomic beam (see Figure 1.3). Atoms emerging from an oven under different angles are first collimated by optical molasses into a parallel beam. This parallel beam is then focused down to a very small spot size by a laser or magnetic lens. In the focus of the lens the transverse velocity of the atoms are again damped by an optical molasses, leading to a very bright atomic beam. In the region between the first optical molasses section and the lens the beam has a very small divergence and in this part of the beamline the atoms can be slowed down using laser slowing. This bright beam can be used to load a trap of atoms, where the atoms can be cooled down further by laser light.

It is instructive to look in more detail for the increase of phase-space density that can be achieved using laser cooling values for rubidium (for a overview of these values for several alkalis and metastable rare gases, see Appendix A). In the first optical molasses section the atoms are collimated in two dimensions from the capture velocity of the molasses (typically  $v_c \approx 5$  m/s) to the Doppler limit  $v_D = 12$  cm/s, which is a compression with a factor 1500. By slowing down the longitudinal velocity of the atoms from thermal velocities  $v_{th} = 350$  m/s to  $v_D$  an additional factor 3000 can be gained. Once the atoms are trapped they can be



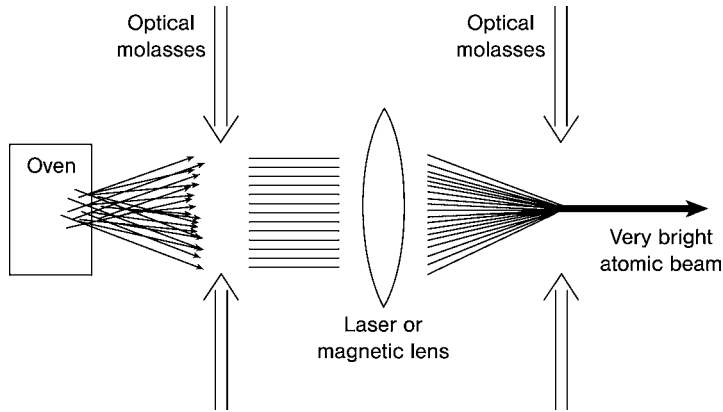


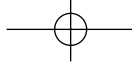
**Figure 1.3** Collimation of an atomic beam using laser cooling techniques.

cooled by sub-Doppler cooling from  $v_D$  to  $v_r = 0.6$  cm/s, yielding another factor 8000. Finally, by creating an optical lattice the atoms can be localized in the potential wells within an optical wavelength, leading to a compression factor of  $10^8$ . Thus, in principle laser cooling and trapping should be able to bridge the gap between phase-space density of a thermal cloud of atoms and atoms in a BEC. However, this analysis assumes that laser cooling and trapping can be applied on all atoms individually, whereas at these temperatures and densities the atoms strongly interact. This causes that the cooling process will no longer be efficient and limits the obtainable temperatures and densities.

In Table 1.3, the different stages of the cooling and trapping of atoms are shown for the experiment of the JILA group, where BEC was observed for the first time [4]. The table shows for this particular experiment which experimental techniques were employed in different stages of the experiment. The total experiment runs about 10 min and in some stages the temperature of the atoms was decreased, whereas in other stages only the density was increased. In the last stage the atoms were

**Table 1.3** The road to BEC, as used in the first experiment to observe BEC [4].

Stages	Action
0	Start in a vapor cell with a background pressure of $10^{-11}$ Torr.
1	Create a dark-spot MOT and collect $10^7$ atoms in 300 s.
2	Cool them to 20 $\mu$ K by adjusting field gradient and laser frequency.
3	Pump them over to the “stretched” state $(F_g, M_g) = (2, 2)$ .
4	Make the TOP trap by switching off the light.
5	Increase quadrupole magnetic field to increase elastic collision rate. Temperature is 90 $\mu$ K and still $4 \times 10^6$ atoms are present. This leads to an elastic collision rate of 3/s, compared to 0.015/s for the background.
6	Evaporative cool for 70 s to 170 nK and $2.5 \times 10^{12}$ atoms/cm <sup>3</sup> . BEC!



cooled evaporatively, which relies on the ejection of the fastest atoms from the trap thereby lowering the temperature of the remaining atoms.

Finally, laser cooling has been discussed as a way to decrease the temperature of a sample of atoms. Lowering the temperature of a sample leads to less disorder in the system and therefore to a decrease of entropy. However, this seems to be in conflict with the second law of thermodynamics, which states that the entropy of a closed system should always increase in time. This apparent contradiction relies on the fact that in laser cooling the atoms do not form a closed system, but interact strongly with the light field. The decrease of entropy of the atoms is accompanied by an increase in entropy of the light field, where the photons in the well-collimated laser beam are scattered in random directions in the spontaneous emission process. Entropy considerations for a laser beam are far from trivial, but recently it has been shown that the entropy decrease of the atoms is many orders of magnitude smaller compared to the entropy increase of the light field.

### 1.3 Doppler Cooling

Laser cooling relies on the exchange of momentum between the light field and the atoms. To describe this process, one has to consider the interaction between the light field and the atoms. Atom-light interaction has been the topic of many textbooks [8–16] and it is not the purpose of this chapter to teach this subject. However, it is worthwhile to consider some of the steps to provide some background for the physics involved. In particular, we will only consider the simplest model of laser cooling, namely Doppler cooling of a two-level atom.

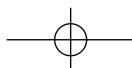
#### 1.3.1 Two-Level Atom in a Light Field

The Hamiltonian for atom–light interaction is given by

$$\mathcal{H}'(t) = -e\vec{\mathcal{E}}(\vec{r}, t) \cdot \vec{r}, \quad (1.3)$$

where the electric component  $\vec{\mathcal{E}}$  of the electromagnetic field interacts with the dipole moment  $\vec{\mu} = -e\vec{r}$  of the atoms. The interaction can be considered as a small perturbation on the total Hamiltonian of the atom and subsequently perturbation theory can be used to calculate the effects of the atom–light interaction on the internal state of the atoms. Since the light field is nearly monochromatic, the light field only couples two states, which we will indicate with  $g$  (ground state) and  $e$  (excited state). Due to the atom–light interaction the amplitudes  $c_{e,g}$  of these states are coupled and the time-derivatives are given by

$$i\hbar \frac{dc_g(t)}{dt} = c_e(t) \mathcal{H}'_{ge}(t) e^{-i\omega_0 t} \quad (1.4)$$



and

$$i\hbar \frac{dc_e(t)}{dt} = c_g(t) \mathcal{H}'_{eg}(t) e^{i\omega_0 t}, \quad (1.5)$$

with  $\mathcal{H}'_{eg}$  the matrix element that couples the ground and excited state through the atom–light interaction. In the case that we can describe the laser field by a traveling plane wave  $\vec{\mathcal{E}}(\vec{r}, t) = E_0 \hat{\epsilon} \cos(kz - \omega t)$ , the atom–light interaction is given in terms of one parameter, the Rabi frequency:

$$\Omega \equiv \frac{-eE_0}{\hbar} \langle e|r|g \rangle. \quad (1.6)$$

This Rabi frequency determines how strongly the field with amplitude  $E_0$  couples the two states in the atoms, which have a dipole moment  $-e\langle e|r|g \rangle$ .<sup>1)</sup> The atom–light interaction causes the amplitudes of ground and excited state to oscillate back and forth with the Rabi frequency  $\Omega$ .

Using the rotating wave approximation, we can write the coherent evolution of the amplitude  $\vec{c} = (c_g, c_e)$  in terms of an effective Hamiltonian:

$$i\hbar \frac{d\vec{c}}{dt} = \mathcal{H}' \vec{c}, \quad (1.7)$$

with

$$\mathcal{H}' = \frac{\hbar}{2} \begin{bmatrix} -2\delta & \Omega \\ \Omega & 0 \end{bmatrix}, \quad (1.8)$$

where  $\delta = \omega - \omega_0$  is the laser detuning from resonance,  $\omega$  is the laser frequency and  $\omega_0$  is the atomic resonance frequency. By diagonalizing this effective Hamiltonian, we obtain the eigenstates of the coupled system. The solution is given by

$$E_{e,g} = \frac{\hbar}{2} (-\delta \mp \Omega'), \quad (1.9)$$

with

$$\Omega' \equiv \sqrt{\Omega^2 + \delta^2}. \quad (1.10)$$

In the limit of  $\Omega \ll |\delta|$  this leads to

$$\Delta E_{g,e} = \pm \frac{\hbar\Omega^2}{4\delta}. \quad (1.11)$$

Depending on the sign of the detuning  $\delta$  of the laser light from resonance the energy of the ground state is shifted upward or downward. This is important in laser traps, where by detuning the laser below resonance atoms can be attracted to the laser focus, or by detuning the laser above resonance repelled from that region. In Figure 1.4 this shift of the energy levels in the atoms has been depicted schematically for a negative detuning.

<sup>1)</sup> Note that the first symbol  $e$  refers to the charge of the electron, whereas the second symbol  $e$  refers to the excited state.

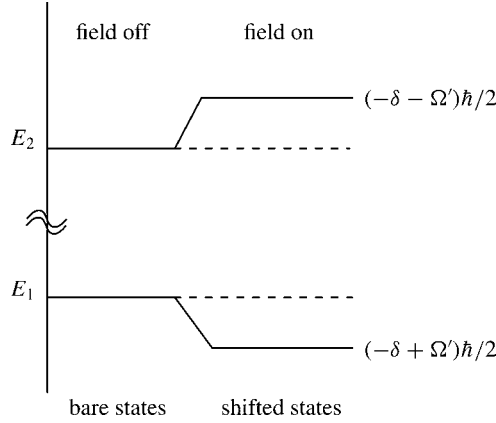


**Figure 1.4** Energies of the two coupled states with the light field off and the light field on. The states are shifted due to the atom–light interaction and the shift is called light shift.

### 1.3.2

#### Optical Bloch Equations

For atom–light interaction the atoms do not form a closed system. We have already discussed this issue in relation to the entropy of the atoms. However, in case of the atom–light interaction this plays a crucial role. So far we have only introduced the two internal states of the atoms and left out the discussion of the light field. It can be shown that by quantizing the light field, we can include the light field in the Hamiltonian and thus obtain a closed system. However, the spontaneous emission process leads to the emission of photons in random directions and thereby lost from the system. This process is irreversible, which accounts for the irreversibility of the cooling process. Since information from the system is lost, we can no longer describe the system in terms of amplitudes and the system has evolved from a pure state to a mixture. Although Eqs. (1.4) and (1.5) still account for coherent evolution of the atomic states in the presence of the light field, it does not account for the spontaneous emission. In order to do so, we will introduce the density matrix to describe the mixed system.

For a pure state, the density matrix is given in terms of the amplitudes  $c_{g,e}$  of the two coupled states as

$$\rho = \begin{pmatrix} \rho_{ee} & \rho_{eg} \\ \rho_{ge} & \rho_{gg} \end{pmatrix} = \begin{pmatrix} c_e c_e^* & c_e c_g^* \\ c_g c_e^* & c_g c_g^* \end{pmatrix}. \quad (1.12)$$

The diagonal element is the probability for the atoms to be in that state, whereas the nondiagonal elements are called the optical coherences. The evolution of the density matrix due to the coherent atom–light interaction is given by

$$i\hbar \frac{d\rho}{dt} = [\mathcal{H}', \rho], \quad (1.13)$$

where the effective Hamiltonian  $\mathcal{H}'$  is given by (1.8). This leads to the so-called optical Bloch equations:

$$\begin{aligned}\frac{d\rho_{gg}}{dt} &= +\gamma\rho_{ee} + \frac{i}{2}(\Omega^*\tilde{\rho}_{eg} - \Omega\tilde{\rho}_{ge}) \\ \frac{d\rho_{ee}}{dt} &= -\gamma\rho_{ee} + \frac{i}{2}(\Omega\tilde{\rho}_{ge} - \Omega^*\tilde{\rho}_{eg}) \\ \frac{d\tilde{\rho}_{ge}}{dt} &= -\left(\frac{\gamma}{2} + i\delta\right)\tilde{\rho}_{ge} + \frac{i}{2}\Omega^*(\rho_{ee} - \rho_{gg}) \\ \frac{d\tilde{\rho}_{eg}}{dt} &= -\left(\frac{\gamma}{2} - i\delta\right)\tilde{\rho}_{eg} + \frac{i}{2}\Omega(\rho_{gg} - \rho_{ee}).\end{aligned}$$

In these equations the terms proportional to the spontaneous decay rate  $\gamma$  have been put in “by hand,” i.e., they have been introduced in the Bloch equations to account for the effects of spontaneous emission. For the ground state the decay of the excited state leads to an increase of the probability  $\rho_{gg}$  to be in the ground state proportional to  $\gamma\rho_{ee}$ , whereas for the excited state it leads to a decrease of  $\rho_{ee}$  proportional to  $\gamma\rho_{ee}$ . These equations have to be solved in order to calculate the force of the laser light on the atoms.

### 1.3.3

#### Steady State

In most cases laser light is applied for a period long compared to the typical evolution times of atom–light interaction, i.e., the lifetime of the excited state  $\tau = 1/\gamma$ . Thus only the steady-state solution of the optical Bloch equations has to be considered. For the probability  $\rho_{ee}$  to be in the excited state the solution is given by

$$\rho_{ee} = \frac{s}{2(1+s)} = \frac{s_0/2}{1+s_0+(2\delta/\gamma)^2}, \quad (1.14)$$

where we have defined the off-resonance saturation parameter  $s$  as

$$s \equiv \frac{|\Omega|^2/2}{\delta^2 + \gamma^2/4} \equiv \frac{s_0}{1+(2\delta/\gamma)^2} \quad (1.15)$$

and the on-resonance saturation parameter  $s_0$  as

$$s_0 \equiv \frac{2|\Omega|^2}{\gamma^2} = \frac{I}{I_s}. \quad (1.16)$$

The probability  $\rho_{ee}$  increases linearly with the saturation parameter  $s$  for small values for  $s$ , but for  $s$  of the order of 1 the probability starts to saturate to a value of  $1/2$ . Thus for very high  $s$  the atom divides its time equally between the ground and excited state. The on-resonance saturation parameters can be expressed in terms of the saturation intensity  $I_s \equiv \pi\hbar c/3\lambda^3\tau$ , where  $I_s$  is typically of the order of a few mW/cm<sup>2</sup> (see Table A.2).

In steady state the atoms cycle between the ground and excited state. In laser cooling the scattering rate of photons from the laser beam is an important parameter, where the absorption of a photon from the light field is followed by spontaneous emission. Since the decay rate of the excited state due to spontaneous emission is given by  $\gamma$ , the scattering rate is given by

$$\gamma_p = \gamma \rho_{ee} = \frac{s_0 \gamma / 2}{1 + s_0 + (2\delta/\gamma)^2}. \quad (1.17)$$

In Figure 1.5, the scattering rate is plotted as a function of detuning for several saturation parameters. For small  $s_0$  the scattering rate is directly proportional to  $s_0$  and the line profile is given by the well-known Lorentz profile. For  $s_0$  in the order of 1 the scattering rate does no longer increase on resonance and obtains its maximal value  $\gamma/2$ . The line profile broadens considerably, since far from resonance the scattering rate is still proportional to  $s_0$ . This effect is referred to as power broadening. The width of the profile is given by  $\gamma' = \gamma \sqrt{1 + s_0}$  and thus for very high  $s_0$  becomes proportional to the square root of  $s_0$ .

### 1.3.4

#### Force on a Two-Level Atom

The force on the atoms due to the atom–light interaction can be calculated by using the Ehrenfest theorem, which states that the force is given by the expectation value of the gradient of the Hamiltonian:

$$F = - \left\langle \frac{\partial \mathcal{H}}{\partial z} \right\rangle. \quad (1.18)$$

This is analogous to the notion that the force on a classical object is given by the gradient of the potential acting on it. For a two-level atom, we can insert the effective Hamiltonian to obtain

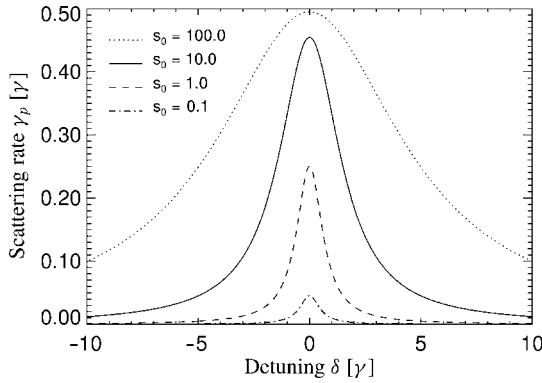


**Figure 1.5** Scattering rate  $\gamma_p$  as a function of the detuning  $\delta$  for several values of the saturation parameter  $s_0$ . Note that for  $s_0 > 1$  the line profiles start to broaden substantially due to power broadening.

$$F = \hbar \left( \frac{\partial \Omega}{\partial z} \rho_{eg}^* + \frac{\partial \Omega^*}{\partial z} \rho_{eg} \right). \quad (1.19)$$

So the force on the atoms only depends on the optical coherences  $\rho_{eg} = \rho_{ge}^*$ . In order to gain some insight in this result, we express the gradient of the Rabi frequency in terms of a real and imaginary part:

$$\frac{\partial \Omega}{\partial z} = (q_r + iq_i)\Omega. \quad (1.20)$$

Although this separation may occur a bit artificial at this stage, we will shortly show that this separation is meaningful. We arrive at the following expression for the force:

$$F = \hbar q_r (\Omega \rho_{eg}^* + \Omega^* \rho_{eg}) + i \hbar q_i (\Omega \rho_{eg}^* - \Omega^* \rho_{eg}). \quad (1.21)$$

The first part of the force is proportional to the real part of the optical coherence and thus proportional to the dispersive part of the atom–light interaction, whereas the second part is proportional to the imaginary part and thus proportional to the absorptive part of the atom–light interaction.

To see, why such a separation is meaningful, consider the interaction of atoms with a traveling plane wave:

$$E(z) = \frac{E_0}{2} \left( e^{i(kz - \omega t)} + \text{c.c.} \right). \quad (1.22)$$

In that case we have  $q_r = 0$  and  $q_i = k$  and the force can only be due to absorption. The force is given by

$$F_{\text{sp}} = \hbar k \gamma \rho_{ee} = \frac{\hbar k s_0 \gamma / 2}{1 + s_0 + (2\delta/\gamma)^2}. \quad (1.23)$$

This force is often called the spontaneous force and can be written as  $F_{\text{sp}} = \hbar k \gamma_p$ , so it is given by the momentum transfer  $\hbar k$  of one absorption of a photon times the scattering rate  $\gamma_p$ . For the case of two traveling plane waves traveling in opposite directions, one has a standing wave and the electric field is given by

$$E(z) = E_0 \cos(kz) \left( e^{-i\omega t} + \text{c.c.} \right). \quad (1.24)$$

Thus we have  $q_r = -k \tan(kz)$  and  $q_i = 0$  and we only retain the dispersive part of the force, which is given by

$$F_{\text{dip}} = \frac{2\hbar k \delta s_0 \sin 2kz}{1 + 4s_0 \cos^2 kz + (2\delta/\gamma)^2}. \quad (1.25)$$

This force is often referred to as dipole force and if one averages this force over a wavelength it averages down to zero. However, this force can be used to trap atoms to dimensions smaller than the wavelength of the light.

## 1.3.5

**Atoms in Motion**

In order to show how these forces can be used to cool atoms, one has to consider the force on atoms, which are in motion. Assuming that the velocity of the atoms is small so that we can treat the velocity  $v$  as a small perturbation on the evolution, the first-order result is given by

$$\frac{d\Omega}{dt} = \frac{\partial\Omega}{\partial t} + v \frac{\partial\Omega}{\partial z} = \frac{\partial\Omega}{\partial t} + v(q_r + iq_i)\Omega. \quad (1.26)$$

Using this expression, we find for the force on a two-level atom in traveling plane wave:

$$F \approx F_0 - \beta v, \quad (1.27)$$

with

$$\beta = -\hbar k^2 \frac{4s_0(\delta/\gamma)}{(1 + s_0 + (2\delta/\gamma)^2)^2}. \quad (1.28)$$

Note that the second term in the force is a true damping force. The damping coefficient  $\beta$  is shown as a function of detuning for several values of  $s_0$  in Figure 1.6. Note that for small  $s_0$  the maximum damping coefficient increases with increasing  $s_0$ , obtains a maximum and decreases for larger values of  $s_0$ . The maximum damping coefficient is given by  $\beta_{\max} = \hbar k^2/4$  and occurs for  $s_0 = 2$  and  $\delta = -\gamma/2$ . Note that the damping rate  $\Gamma$  is proportional to the damping coefficient, namely  $\Gamma \equiv \beta/M$  and thus the maximum damping rate is given by  $\Gamma_{\max} = \hbar k^2/4M = \omega_r/2$ . For most atoms this damping rate leads to a damping time, which is of the order of tens of  $\mu\text{s}$ . Note that the constant term  $F_0$  in (1.27) leads to a cooling of the atoms to a nonzero velocity of  $v = F_0/\beta$ , but by using two counterpropagating laser beams the constant term can be cancelled (see Section 1.5).

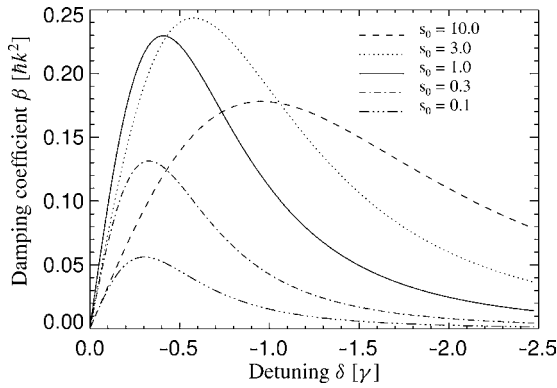


**Figure 1.6** The damping coefficient  $\beta$  for atoms in a traveling wave as a function of detuning for different values of the saturation parameter  $s_0$ . The damping coefficient is maximum for intermediate detunings and intensities.



## 1.4 Laser Slowing

### 1.4.1 Introduction

The origin of optical forces on atoms has been discussed in Section 1.3.4, and here a specific application is introduced. The use of electromagnetic forces to influence the motion of neutral atoms has been a subject of interest for some years [17–21]. The force caused by radiation, particularly by light at or near the resonance frequencies of atomic transitions, originates from the momentum associated with light. In addition to energy  $E = \hbar\omega$ , each photon carries momentum  $\hbar k$  and angular momentum  $\hbar$ . When an atom absorbs light, it stores the energy by going into an excited state; it stores the momentum by recoiling from the light source with a momentum  $\hbar k$ ; and it stores the angular momentum in the form of internal motion of its electrons (see Figure 1.7). The converse applies for emission, whether it is stimulated or spontaneous. It is the velocity change of the atoms,  $v_r = \hbar k/M \simeq$  few cm/s that is of special interest here, and although it is very small compared with thermal velocity, multiple absorptions can be used to produce a large total velocity change. Proper control of this velocity change constitutes a radiative force that can be used to decelerate and/or to cool free atoms.

Although there are many ways to decelerate and cool atoms from room temperature or higher, the one that has received the most attention by far depends on the scattering force that uses this momentum transfer between the atoms and a radiation field resonant with an atomic transition. By making a careful choice of geometry and of the light frequency one can exploit the Doppler shift to make the momentum exchange (hence the force) velocity dependent. Because the force is velocity dependent, it can not only be used for deceleration, but also for cooling, which results in increased phase-space density (see Section 1.2).

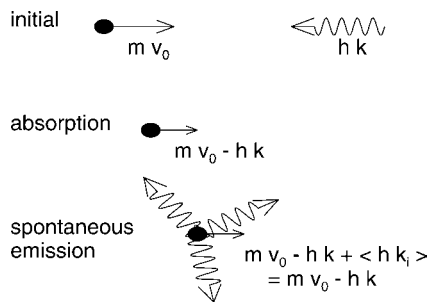


**Figure 1.7** Schematic diagram for the pressure of light on atoms. Initially the atom has a momentum  $m v_0$  and the photon has a momentum  $\hbar k$  in the opposite direction. Once the light is absorbed, the momentum of the atom is reduced to  $m v_0 - \hbar k$ . In the next step light is emitted in a random

direction and the recoil of the photon on the atom averages over a large number of cycles out to zero. The final momentum of the atom is thus on the average reduced during an absorption and spontaneous emission cycle.

## 1.4.2

**Slowing of an Atomic Beam**

The idea that the radiation scattering force on free atoms could be velocity dependent and therefore be used for cooling a gas was suggested by Wineland and Dehmelt [1], Hansch and Schawlow [2], and Wineland and Itano [22], although Kastler, Landau, and others had made allusions to it in earlier years. The possibility for cooling stems from the fact that atomic absorption of light near a resonance is strongly frequency dependent, and is therefore velocity dependent because of the Doppler shift of the laser frequency seen by the atoms moving relative to the laboratory-fixed laser. Of course, a velocity-dependent dissipative force is needed for cooling.

One very obvious implementation of radiative deceleration and cooling is to direct a laser beam opposite to an atomic beam as shown in Figure 1.8 [23, 24]. In this case each atom can absorb light many times along its path through the apparatus. Of course, excited-state atoms cannot absorb light efficiently from the laser that excited them, so between absorptions they must return to the ground state by spontaneous decay, accompanied by emission of fluorescent light. The emitted fluorescent light will also change the momentum of the atoms, but its spatial symmetry results in an average of zero net momentum transfer after many such fluorescence events. So the net deceleration of the atoms is in the direction of the laser beam, and the maximum deceleration is limited by the spontaneous fluorescence rate.

The maximum attainable deceleration is obtained for very high light intensities, and is limited because the atom must then divide its time equally between ground and excited states. High-intensity light can produce faster absorption, but it also causes equally fast stimulated emission; the combination produces neither deceleration nor cooling because the momentum transfer to the atom in emission is then in the opposite direction to what it was in absorption. The deceleration

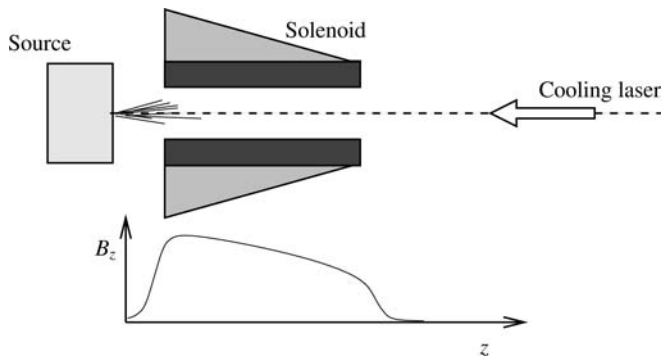


**Figure 1.8** Schematic diagram of apparatus for beam slowing. The tapered magnetic field is produced by layers of varying length on the solenoid. A plot of  $B_z$  versus  $z$  is also shown.

therefore saturates at a value  $\vec{a}_{\max} = \hbar\vec{k}\gamma/2M$ , where the factor of 2 arises because the atoms spend half of their time in each state.

The Doppler shifted laser frequency in the moving atoms' reference frame should match that of the atomic transition to maximize the light absorption and scattering rate. This rate  $\gamma_p$  is given by the Lorentzian (see Eq. (1.17))

$$\gamma_p = \frac{s_0\gamma/2}{1 + s_0 + [2(\delta + \omega_D)/\gamma]^2}, \quad (1.29)$$

where  $s_0$  is defined in (1.16). The Doppler shift seen by the moving atoms is  $\omega_D = -\vec{k} \cdot \vec{v}$  (note that  $\vec{k}$  opposite to  $\vec{v}$  produces a positive Doppler shift). Maximum deceleration requires  $(\delta + \omega_D) \ll \gamma$ , so that the laser light is nearly resonant with the atoms in their rest frame. The net force on the atoms is  $\vec{F} = \hbar\vec{k}\gamma_p$  (see Eq. (1.23)), which saturates at large  $s_0$  to  $M\vec{a}_{\max} = \vec{F}_{\max} \equiv \hbar\vec{k}\gamma/2$ .

Table 1.4 shows some of the parameters for slowing a few atomic species of interest from the peak of the thermal velocity distribution. Since the maximum deceleration  $\vec{a}_{\max}$  is fixed by atomic parameters, it is straightforward to calculate the minimum stopping length  $L_{\min}$  and time  $t_{\min}$  for the rms velocity of atoms  $\bar{v} = 2\sqrt{k_B T/M}$  at the chosen temperature. The result is  $L_{\min} = \bar{v}^2/2a_{\max}$  and  $t_{\min} = \bar{v}/a_{\max}$ . It is comforting to note that  $|\vec{F}_{\max}|L_{\min}$  is just the atomic kinetic energy and that  $L_{\min}$  is just  $t_{\min}\bar{v}/2$ .

If the light source is spectrally narrow, then as the atoms in the beam slow down, their changing Doppler shift will take them out of resonance. They will eventually cease deceleration after their Doppler shift has been decreased by a few times the power-broadened width  $\gamma' = \gamma\sqrt{1 + s_0}$  as derived from (1.17), corresponding to  $\Delta v$  of a few times  $\gamma/k$ . Although this  $\Delta v$  of a few m/s is considerably larger than the typical atomic recoil velocity  $v_r$  of a few cm/s, it is still only a small fraction of the

Table 1.4 Parameters of interest for slowing various atoms.<sup>a</sup>

Atom	$T_{\text{oven}}$ (K)	$\bar{v}$ (m/s)	$L_{\min}$ (m)	$t_{\min}$ (ms)
H	1000	5000	0.012	0.005
He*	4	158	0.03	0.34
He*	650	2013	4.4	4.4
Li	1017	2051	1.15	1.12
Na	712	876	0.42	0.96
K	617	626	0.77	2.45
Rb	568	402	0.75	3.72
Cs	544	319	0.93	5.82

<sup>a</sup>The stopping length  $L_{\min}$  and time  $t_{\min}$  are minimum values. The oven temperature  $T_{\text{oven}}$  that determines the peak velocity is chosen to give a vapor pressure of 1 Torr. Special cases are H at 1000 K and He in the metastable triplet state, for which two rows are shown: one for a 4 K source and another for the typical discharge temperature.

atoms' average thermal velocity, so that significant further cooling or deceleration cannot be accomplished.

In order to accomplish deceleration that changes the atomic speeds by hundreds of m/s, it is necessary to maintain  $(\delta + \omega_D) \ll \gamma$  by compensating such changes of the Doppler shift. This can be done by changing  $\omega_D$ , or  $\delta$  via either  $\omega$  or  $\omega_0$ . The most common method for overcoming this problem is spatially varying the atomic resonance frequency with an inhomogeneous dc magnetic field to keep the decelerating atoms in resonance with the fixed frequency laser [23, 25].

### 1.4.3

#### **Zeeman-Compensated Slowing**

The use of a spatially varying magnetic field to tune the atomic levels along the beam path was the first method to succeed in slowing atoms [23]. It works as long as the Zeeman shifts of the ground and excited states are different so that the resonant frequency is shifted. The field can be tailored to provide the appropriate Doppler shift along the moving atom's path. For uniform deceleration  $a \equiv \eta a_{\max}$  from initial velocity  $v_0$ , the appropriate field profile is

$$B(z) = B_0 \sqrt{1 - z/z_0}, \quad (1.30)$$

where  $z_0 \equiv Mv_0^2/\eta\hbar k\gamma$  is the length of the magnet,  $B_0 = \hbar kv_0/\mu'$ ,  $\mu' \equiv (g_e M_e - g_g M_g)\mu_B$ , subscripts  $g$  and  $e$  refer to ground and excited states, respectively,  $g_{g,e}$  is the Landé  $g$ -factor,  $\mu_B$  is the Bohr magneton, and  $M_{g,e}$  is the magnetic quantum number. The design parameter  $\eta < 1$  determines the length of the magnet  $z_0$ . A solenoid that can produce such a spatially varying field has layers of decreasing lengths as shown schematically in Figure 1.8. The technical problem of extracting the beam of slow atoms from the end of the solenoid can be simplified by reversing the field gradient and choosing a transition whose frequency decreases with increasing field [26].

The equation of motion of atoms in the magnet cannot be easily solved in general because of the velocity-dependent force, but by transforming to a decelerating frame  $\mathcal{R}$  [27] the problem can be addressed. For the special case of uniform deceleration the velocity of this frame in the lab is  $v_{\mathcal{R}} = v_0 \sqrt{1 - z/z_0}$ , and the Doppler shift associated with this velocity is compensated by the position-dependent Zeeman shift in the magnet. The resulting equation of motion for the velocity of atoms  $v' \equiv v - v_{\mathcal{R}}$  relative to this frame is given by

$$M \frac{d\vec{v}'}{dt} = -\vec{F}_{\max} \left[ \frac{s_0}{1 + s_0 + \left(2(\delta - \vec{k} \cdot \vec{v}')/\gamma\right)^2} - \eta \right], \quad (1.31)$$

where  $\vec{F}_{\max} = \hbar \vec{k} \gamma / 2$ . For  $dv'/dt = 0$  the steady-state velocity  $v'_{ss}$  is given by

$$kv'_{ss} = \delta \pm \frac{\gamma}{2} \sqrt{s_0 \frac{1 - \eta}{\eta}} - 1. \quad (1.32)$$

There are two values of  $v'_{ss}$  but the one with the (+) sign is unstable. The magnitude of  $v'_{ss}$  is typically of order  $\delta/k$ . This velocity is approximately constant as atoms decelerate along their paths through the magnet so the decreasing Doppler shift is compensated by the decreasing Zeeman shifts.

#### 1.4.4

##### Measurements and Results

This section presents some results of experiments that used the Zeeman tuning technique to compensate the changing Doppler shift. The most common way to measure the slowed velocity distribution is to detect the fluorescence from atoms excited by a second laser beam propagating at a small angle to the atomic beam [23]. Because of the Doppler shift, the frequency dependence of this fluorescence provides a measure of the atomic velocity distribution. In this method, the velocity resolution  $\Delta v$  is limited by the natural width of the excited state to  $\Delta v = \gamma/k$  ( $\approx 6$  m/s for Na).

In 1997, a new time-of-flight (TOF) method to accomplish the same result was reported, however, with a much improved resolution [28]. In addition, it provided a much more powerful diagnostic of the deceleration process. The TOF method has the capability to map out the velocity distribution for both hyperfine ground states of alkali atoms along their entire path through the solenoid. The experimental arrangement is shown in Figure 1.9. The atoms emerge through an aperture of  $1 \text{ mm}^2$  from an effusive Na source heated to approximately  $300^\circ\text{C}$ . During their subsequent flight through a solenoid, they are slowed by the counterpropagating laser light from laser 2, and the changing Doppler shift is compensated with a field that is well described by (1.30).

For the TOF technique there are two additional beams labeled pump and probe as shown in Figure 1.9. Because these beams cross the atomic beam at  $90^\circ$ ,  $\vec{k} \cdot \vec{v} = 0$  and they excite atoms at all velocities. The pump beam is tuned to excite and empty a selected ground hyperfine state (hfs), and it transfers more than 98% of

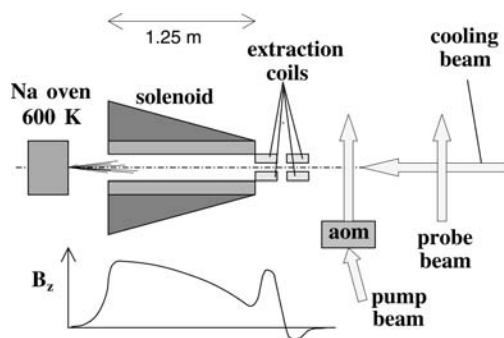


**Figure 1.9** The TOF apparatus, showing the solenoid magnet and the location of the two laser beams used as the pump and probe.

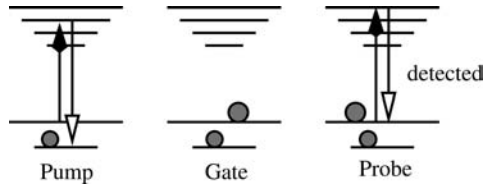


**Figure 1.10** Schematic diagram of the optical pumping process that is used to measure the velocity of the atoms by TOF. The pump beam pumps all the atoms toward the lowest hyperfine ground state. Shortly interrupting the pump beam then acts as a gate,

leaving the atoms in the upper hyperfine ground state. The arrival time of those atoms at the position of the probe is measured using fluorescence detection and this is a measure of the atomic velocity.

the population as the atoms pass through its 0.5 mm width (see Figure 1.10). To measure the velocity distribution of atoms in the selected hfs, this pump laser beam is interrupted for a period  $\Delta t = 10\text{--}50\ \mu\text{s}$  with an acoustic optical modulator (AOM). A pulse of atoms in the selected hfs passes the pump region and travels to the probe beam. The time dependence of the fluorescence induced by the probe laser, tuned to excite the selected hfs, gives the time of arrival, and this signal is readily converted to a velocity distribution. Figure 1.11 shows the measured velocity distribution of the atoms slowed by the cooling laser.

With this TOF technique, the resolution is limited by the duration of the pump laser gate  $\Delta t$  and the diameter  $d$  of the probe laser beam ( $d \leq 1.0\ \text{mm}$ ) to  $\Delta v = v(\Delta t + d)/z_p$ , typically less than 1 m/s. This provides the capability of measuring the shape of the velocity distribution with resolution  $\approx 10$  times better

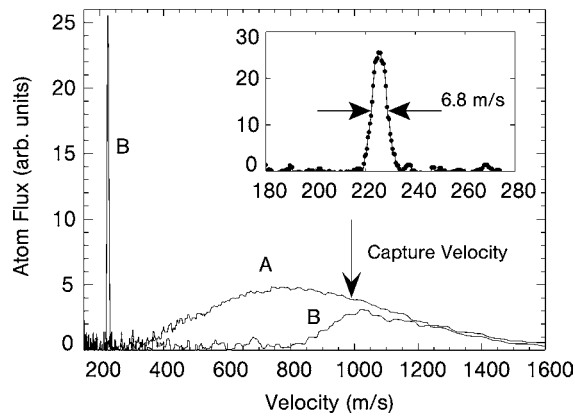


**Figure 1.11** The velocity distribution measured with the TOF method. Trace A shows the velocity distribution of atoms from the oven, where the cooling beam is blocked. The distribution is a typical Maxwell–Boltzmann distribution with a temperature of 500 K. Trace B shows the

velocity distribution, when the cooling laser starts to cool atoms down from about 1000 m/s. All atoms below this velocity are slowed down to 220 m/s. The inset shows an enlargement of the velocities around 220 m/s, showing that the width of the distribution is about 6.8 m/s.

than  $\gamma/k$  as compared with the Doppler method. Furthermore, the resolution improves for decreasing velocity  $v$ ;  $\Delta v$  is smaller than the Doppler cooling limit of  $\sqrt{\hbar\gamma/2M} \approx 30$  cm/s for  $v \approx 80$  m/s and Na atoms. Figure 1.11 shows the final velocity distribution for such a measurement giving a FWHM of 3.0 m/s at a central velocity of 138 m/s. The width is about one half of  $\gamma/k$ .

The method of shutting off the slowing laser beam a variable time  $\tau_{\text{off}}$  before the short shut-off of the pump beam offers a much more informative scheme of data acquisition. The atoms that pass through the pump region during the short time when the pump beam is off have already traveled a distance  $\Delta z = v(z)\tau_{\text{off}}$  (at constant velocity  $v(z)$  because the slowing laser was off), and their time of arrival at the probe laser is  $z_p/v(z) = z_p\tau_{\text{off}}/\Delta z$ . Thus the TOF signal contains information not only about the velocity of the detected atoms, but also about their position  $z$  in the magnet at the time the slowing laser light was shut off. Since the spatial

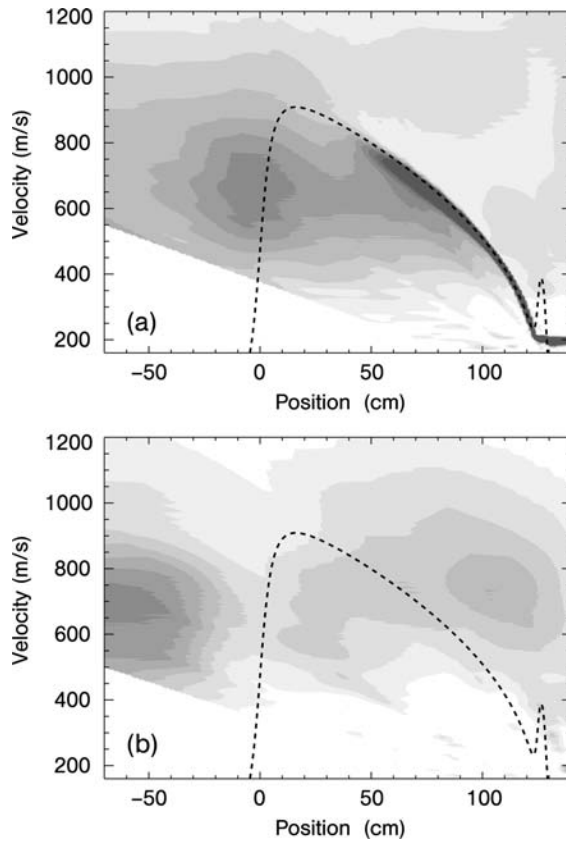
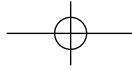


**Figure 1.12** Contour map of the measured velocity and position of atoms in the solenoid, (a) for  $F_g = 2$  atoms and (b) for  $F_g = 1$  atoms. The dashed line indicates the resonance frequency for the  $(F, M_F) = (2,$

$2) \rightarrow (3, 3)$  cycling transition. The density of atoms per unit phase-space area  $\Delta v \Delta z$  has been indicated with different gray levels (figure from Ref. [28]).



dependence of the magnetic field is known (Figure 1.8), both the field and atomic velocity at that position can be determined, and the TOF signal is proportional to the number of atoms in that particular region of phase space. This new technique therefore gives a mapping of the atomic population in the  $z$ -direction of the phase space,  $z$  and  $v(z)$ , within the solenoid.

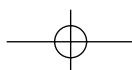
Such mapping of the velocity distribution within the solenoid is a powerful diagnostic tool. The contours of Figures 1.12(a) and (b) represent the strength of the TOF signal for each of the two hfs levels, and thus the density of atoms, at each velocity and position in the magnet. The dashed line shows the velocity  $v(z) = (\mu' B(z)/\hbar - \delta)/k$  for which the magnetic field tunes the atomic transition  $(F, M_F) = (2, 2) \rightarrow (3, 3)$  into resonance with the decelerating beam. The most obvious new information in Figure 1.12(a) is that atoms are strongly concentrated at velocities just below that of the resonance condition. This corresponds to the strong peak of slow atoms shown in Figure 1.11.

## 1.5 Laser Cooling

### 1.5.1 Optical Molasses

Section 1.4 presented a discussion of the radiative force on atoms moving in a single laser beam. Here this notion is extended to include the radiative force from more than just one beam. For example, if two low-intensity laser beams of the same frequency, intensity, and polarization are directed opposite to one another (e.g., by retroreflection of a single beam from a mirror), the net force found by adding the radiative forces given in (1.23) from each of the two beams obviously vanishes for atoms at rest because  $\vec{k}$  is opposite for the two beams. However, atoms moving slowly along the light beams experience a net force proportional to their velocity whose sign depends on the laser frequency. If the laser is tuned below atomic resonance, the frequency of the light in the beam opposing the atomic motion is Doppler shifted toward the blue in the atomic rest frame, and is therefore closer to resonance; similarly, the light in the beam moving parallel to the atom will be shifted toward the red, further out of resonance (see Figure 1.13). Atoms will therefore interact more strongly with the laser beam that opposes their velocity and they will slow down. This is illustrated in Figure 1.14.

The slowing force is proportional to velocity for small enough velocities, resulting in viscous damping [29, 30] as shown in Eq. (1.27) that gives this technique the name “optical molasses” (OM). By using three intersecting orthogonal pairs of oppositely directed beams, the movement of atoms in the intersection region can be severely restricted in all three dimensions, and many atoms can thereby be collected and cooled in a small volume. OM has been demonstrated at several laboratories [31], often with the use of low-cost diode lasers [32].





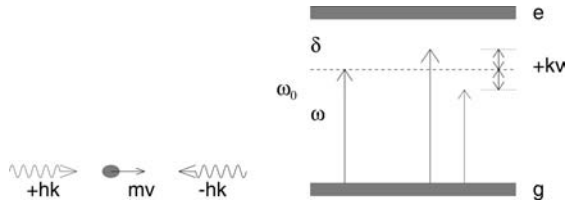


**Figure 1.13** Standard configuration for laser cooling in an optical molasses. By detuning the laser frequency  $\omega$  below the resonance frequency  $\omega_0$  the frequency of the laser opposing the atomic motion is shifted toward resonance, whereas the frequency of the other laser beam is shifted out of resonance.

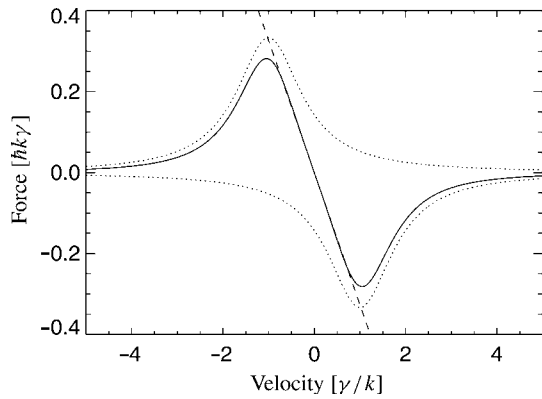


**Figure 1.14** Velocity dependence of the optical damping forces for one-dimensional optical molasses. The two dotted traces show the force from each beam, and the solid curve is their sum. The straight line shows how this force mimics a pure damping force over a restricted velocity range. These are calculated for  $s_0 = 2$  and  $\delta = -\gamma$  so there is some power broadening evident (see Section 1.3.3).

Note that OM is not a trap for neutral atoms because there is no restoring force on atoms that have been displaced from the center. Still, the detainment times of atoms caught in OM of several mm diameter can be remarkably long. It can be very instructive to carry out your own experiment at home. For this experiment the only thing that is needed is a jar of molasses (Deutsch, der Sirup; français, mélasse; English, syrup; nederlands, stroop; lingua latina, mellaceus; italiano, melassa; espanol, melaza; ελληνικός, μελασσα) and a marble. By throwing the marble in the molasses one can witness the extraordinary ability of the molasses to damp the velocity of the marble. If one tries to move the marble around, its motion will be strongly damped by the thick and sticky molasses.

## 1.5.2

**Low-Intensity Theory for a Two-Level Atom in One Dimension**

It is straightforward to estimate the force on atoms in OM from (1.23). The discussion here is limited to the case where the light intensity is low enough so that stimulated emission is not important. This eliminates consideration of excitation of an atom by light from one beam and stimulated emission by light from the other, a sequence that can lead to very large, velocity-independent changes in the atom's speed. In this low-intensity case, the forces from the two light beams are simply added to give  $\vec{F}_{\text{OM}} = \vec{F}_+ + \vec{F}_-$ , where

$$\vec{F}_{\pm} = \pm \frac{\hbar k \gamma}{2} \frac{s_0}{1 + s_0 + [2(\delta \mp |\omega_{\text{D}}|)/\gamma]^2}. \quad (1.33)$$

Then the sum of the two forces is

$$\vec{F}_{\text{OM}} \cong \frac{8\hbar k^2 \delta s_0 \vec{v}}{\gamma(1 + s_0 + (2\delta/\gamma)^2)} \equiv -\beta \vec{v}, \quad (1.34)$$

where terms of order  $(kv/\gamma)^4$  and higher have been neglected (see (1.27)). For  $\delta < 0$ , this force opposes the velocity and therefore viscously damps the atomic motion. For large  $\delta$ , the force  $\vec{F}_{\text{OM}}$  has maxima near  $v = \pm\delta/k$  as expected.

If there were no other influence on the atomic motion, all atoms would quickly decelerate to  $v = 0$  and the sample would reach  $T = 0$ , a clearly unphysical result. There is also some heating caused by the light beams that must be considered, and it derives from the discrete size of the momentum steps the atoms undergo with each emission or absorption. Since the atomic momentum changes by  $\hbar k$ , their kinetic energy changes on the average by at least the recoil energy  $E_r = \hbar^2 k^2 / 2M = \hbar \omega_r$ . This means that the average frequency of each absorption is  $\omega_{\text{abs}} = \omega_0 + \omega_r$  and the average frequency of each emission is  $\omega_{\text{emit}} = \omega_0 - \omega_r$ . Thus the light field loses an average energy of  $\hbar(\omega_{\text{abs}} - \omega_{\text{emit}}) = 2\hbar\omega_r$  for each scattering. This loss occurs at a rate  $2\gamma_p$  (two beams), and the energy becomes atomic kinetic energy because the atoms recoil from each event. The atomic sample is thereby heated because these recoils are in random directions.

The competition between this heating with the damping force of (1.34) results in a nonzero kinetic energy in steady state. At steady state, the rates of heating and cooling for atoms in OM are equal. Equating the cooling rate,  $\vec{F} \cdot \vec{v}$ , to the heating rate,  $4\hbar\omega_r\gamma_p$ , the steady-state kinetic energy is found to be  $(\hbar\gamma/8)(2|\delta|/\gamma + \gamma/2|\delta|)$ . This result is dependent on  $|\delta|$ , and it has a minimum at  $2|\delta|/\gamma = 1$ , whence  $\delta = -\gamma/2$ . The temperature found from the kinetic energy is then  $T_{\text{D}} = \hbar\gamma/2k_{\text{B}}$ , where  $k_{\text{B}}$  is Boltzmann's constant and  $T_{\text{D}}$  is called the Doppler temperature or the Doppler cooling limit. For ordinary atomic transitions  $T_{\text{D}}$  is below 1 mK, and several typical values are given in Table A.3 (see Appendix A).

Another instructive way to determine  $T_{\text{D}}$  is to note that the average momentum transfer of many spontaneous emissions is zero, but the rms scatter of these about zero is finite. One can imagine these decays as causing a random walk in momentum space with step size  $\hbar k$  and step frequency  $2\gamma_p$ , where the factor

of 2 arises because of the two beams. The random walk results in diffusion in momentum space with diffusion coefficient  $D_0 \equiv 2(\Delta p)^2/\Delta t = 4\gamma_p(\hbar k)^2$ . Then Brownian motion theory gives the steady-state temperature in terms of the damping coefficient  $\beta$  to be  $k_B T = D_0/\beta$ . This turns out to be  $\hbar\gamma/2$  as above for the case  $s_0 \ll 1$  when  $\delta = -\gamma/2$ . There are many other independent ways to derive this remarkable result that predicts that the final temperature of atoms in OM is independent of the optical wavelength, atomic mass, and laser intensity (as long as it is not too large).

### 1.5.3

#### Experiments in Three-Dimensional Optical Molasses

Optical molasses experiments can also work in three dimensions at the intersection of three mutually orthogonal pairs of opposing laser beams (see Ref. [18]). Even though atoms can be collected and cooled in the intersection region, it is important to stress again that this is *not* a trap. That is, atoms that wander away from the center experience no force directing them back. They are allowed to diffuse freely and even escape, as long as there is enough time for their very slow diffusive movement to allow them to reach the edge of the region of the intersection of the laser beams. Because the atomic velocities are randomized during the damping time  $1/\omega_r$ , atoms execute a random walk with a step size of  $v_D/\omega_r = \lambda/2\pi\sqrt{2\varepsilon} \cong$  few  $\mu\text{m}$ . To diffuse a distance of 1 cm requires about  $10^7$  steps or about 30 s [33, 34].

Three-dimensional OM was first observed in 1985 [30]. Preliminary measurements of the average kinetic energy of the atoms were done by blinking off the laser beams for a fixed interval. Comparison of the brightness of the fluorescence before and after the turnoff was used to calculate the fraction of atoms that left the region while it was in the dark. The dependence of this fraction on the duration of the dark interval was used to estimate the velocity distribution and hence the temperature. The result was not inconsistent with the two-level atom theory described in Section. 1.5.2.

Soon other laboratories had produced 3D OM. The photograph in Figure 1.15 shows OM in Na at the laboratory in the National Bureau of Standards (now NIST) in Gaithersburg. The phenomenon is readily visible to the unaided eye, and the photograph was made under ordinary snapshot conditions. The three mutually perpendicular pairs of laser beams appear as a star because they are viewed along a diagonal.

This NIST group developed a more accurate ballistic method to measure the velocity distribution of atoms in OM [36]. The limitation of the first measurements was determined by the size of the OM region and the unknown spatial distribution of atoms [30]. The new method at NIST used a separate measuring region composed of a 1D OM about 2 cm below the 3D region, thereby reducing the effect of this limitation. When the laser beams forming the 3D OM were shut off, the atoms dropped because of gravity into the 1D region, and the time-of-arrival distribution was measured. This was compared with calculated distributions for  $T_D$  and 40  $\mu\text{K}$  as shown in Figure 1.16. Using a series of plots like Figure 1.16 it was possible

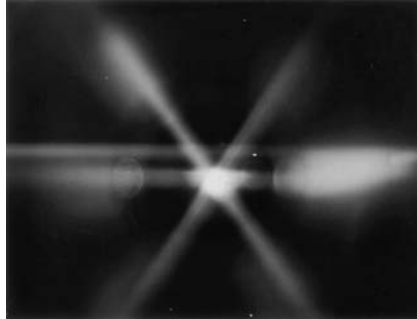


**Figure 1.15** Photograph of optical molasses in Na taken under ordinary snapshot conditions in the lab at NIST. The upper horizontal streak is from the slowing laser while the three beams that cross at the center are

on mutually orthogonal axes viewed from the (111) direction. Atoms in the optical molasses glow brightly at the center (figure from Ref. [35]).

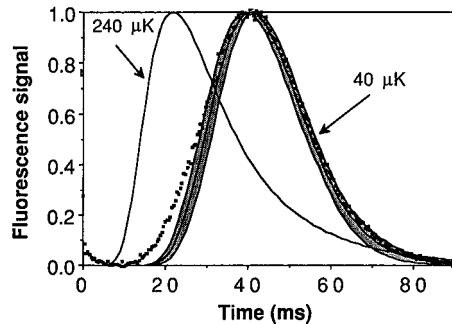


**Figure 1.16** Data from dropping atoms out of optical molasses into a probe beam about 18 mm below. The calculated TOF spectra are for 240 and 40  $\mu\text{K}$ . The shaded area indicates the range of error in the 40  $\mu\text{K}$

calculation from geometric uncertainties. The width of the data is slightly larger than the calculation, presumably because of shot-to-shot instabilities (figure from Ref. [36]).

to determine the dependence of temperature on detuning, and that is shown in Figure 1.17, along with the theoretical calculations for a two-level atom, as given in Section 1.5.2.

It was an enormous surprise to observe that the ballistically measured temperature of the Na atoms was as much as 10 times *lower* than  $T_D = 240 \mu\text{K}$  [36], the temperature minimum calculated from the theory. This breaching of the Doppler limit forced the development of an entirely new picture of OM that accounts for the fact that in 3D, a two-level picture of atomic structure is inadequate. The multilevel structure of atomic states, and optical pumping among these sublevels, must be considered in the description of 3D OM, as discussed in Section 1.7.

These experiments also found that OM was less sensitive to perturbations and more tolerant of alignment errors than was predicted by the 1D, two-level atom theory. For example, if the intensities of the two counterpropagating laser beams forming an OM were unequal, then the force on atoms at rest would not vanish,

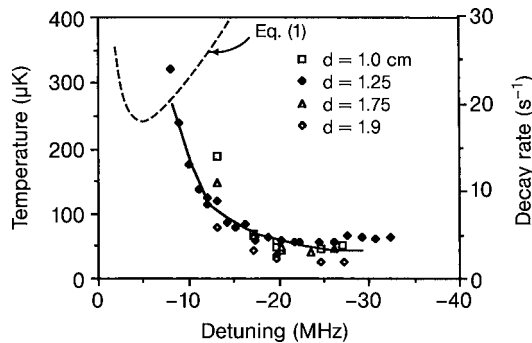


**Figure 1.17** Temperature versus detuning determined from time-of-flight data for various separations  $d$  between the optical molasses and the probe laser (data points). The solid curve represents the measured molasses decay rate; it is not a fit to the temperature data points, but its scale (shown at right) was chosen to emphasize its proportionality to the temperature data. The dashed line shows the temperature expected on the basis of the two-level atom theory of Section 1.5.2 (figure from Ref. [36]).

but the force on atoms with some nonzero drift velocity *would* vanish. This drift velocity can be easily calculated by using (1.33) with unequal intensities  $s_{0+}$  and  $s_{0-}$ , and following the derivation of (1.34). Thus atoms would drift out of an OM, and the calculated rate would be much faster than observed by deliberately unbalancing the beams in the experiments [31].

Section 1.7 describes the startling new view of OM that emerged in the late 1980s as a result of these surprising measurements. The need for a new theoretical description resulting from incontrovertible measurements provides an excellent pedagogical example of how physics is truly an experimental science, depending on the interactions between observations and theory, and always prepared to discard oversimplified descriptions as soon as it is shown that they are inadequate.

## 1.6 Magneto-Optical Traps

### 1.6.1 Introduction

The most widely used trap for neutral atoms is a hybrid, employing both optical and magnetic fields, to make a magneto-optical trap (MOT) first demonstrated in 1987 [37]. The operation of an MOT depends on both inhomogeneous magnetic fields and radiative selection rules to exploit both optical pumping and the strong radiative force [37, 38]. The radiative interaction provides cooling that helps in loading the trap, and enables very easy operation. The MOT is a very robust trap that does not depend on precise balancing of the counterpropagating laser beams or on a very high degree of polarization. The magnetic field gradients are modest and can readily be achieved with simple, air-cooled coils. The trap is easy to construct

because it can be operated with a room-temperature cell, where alkali atoms are captured from the vapor. Furthermore, low-cost diode lasers can be used to produce the light appropriate for all the alkalis except Na, so the MOT has become one of the least expensive ways to produce atomic samples with temperatures below 1 mK.

Trapping in an MOT works by optical pumping of slowly moving atoms in a linearly inhomogeneous magnetic field  $B = B(z) \equiv Az$ , such as that formed by a magnetic quadrupole field as discussed in Section 1.8. Atomic transitions with the simple scheme of  $J_g = 0 \rightarrow J_e = 1$  have three Zeeman components in a magnetic field, excited by each of three polarizations, whose frequencies tune with field (and therefore with position) as shown in Figure 1.18 for 1D. Two counterpropagating laser beams of opposite circular polarization, each detuned below the zero-field atomic resonance by  $\delta$ , are incident as shown.

Because of the Zeeman shift, the excited state  $M_e = +1$  is shifted up for  $B > 0$ , whereas the state with  $M_e = -1$  is shifted down. At position  $z'$  in Figure 1.18 the magnetic field therefore tunes the  $\Delta M = -1$  transition closer to resonance and the  $\Delta M = +1$  transition further out of resonance. If the polarization of the laser beam incident from the right is chosen to be  $\sigma^-$  and correspondingly  $\sigma^+$  for the other beam, then more light is scattered from the  $\sigma^-$  beam than from the  $\sigma^+$  beam. Thus the atoms are driven toward the center of the trap where the magnetic field is zero. On the other side of the center of the trap, the roles of the  $M_e = \pm 1$  states are reversed and now more light is scattered from the  $\sigma^+$  beam, again driving the atoms toward the center.

The situation is analogous to the velocity damping in an optical molasses from the Doppler effect as discussed in Section 1.5.2, but here the effect operates in

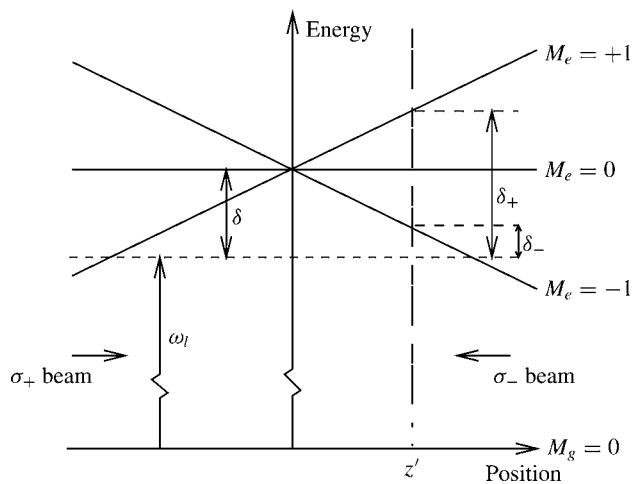


**Figure 1.18** Arrangement for a MOT in 1D. The horizontal dashed line represents the laser frequency seen by atoms at rest in the center of the trap. Because of the Zeeman shifts of the atomic transition frequencies in the inhomogeneous magnetic field, atoms at  $z = z'$  are closer to resonance with the  $\sigma^-$  laser beam than with the  $\sigma^+$  beam, and are therefore driven toward the center of the trap.

position space, whereas for molasses it operates in velocity space. Since the laser light is detuned below the atomic resonance in both the cases, compression and cooling of the atoms is obtained simultaneously in an MOT.

So far the discussion has been limited to the motion of atoms in 1D. However, the MOT scheme can easily be extended to 3D by using six instead of two laser beams. Furthermore, even though very few atomic species have transitions as simple as  $J_g = 0 \rightarrow J_e = 1$ , the scheme works for any  $J_g \rightarrow J_e = J_g + 1$  transition. Atoms that scatter mainly from the  $\sigma^+$  laser beam will be optically pumped toward the  $M_g = +J_g$  substate, which forms a closed system with the  $M_e = +J_e$  substate.

### 1.6.2

#### Cooling and Compressing Atoms in an MOT

For a description of the motion of the atoms in an MOT, consider the radiative force in the low-intensity limit (see Eq. (1.23)). The total force on the atoms is given by  $\vec{F} = \vec{F}_+ + \vec{F}_-$ , where

$$\vec{F}_\pm = \pm \frac{\hbar \vec{k} \gamma}{2} \frac{s_0}{1 + s_0 + (2\delta_\pm/\gamma)^2} \quad (1.35)$$

and the detuning  $\delta_\pm$  for each laser beam is given by

$$\delta_\pm = \delta \mp \vec{k} \cdot \vec{v} \pm \mu' B/\hbar. \quad (1.36)$$

Here  $\mu' \equiv (g_e M_e - g_g M_g) \mu_B$  is the effective magnetic moment for the transition used (see Section 1.4.3). Note that the Doppler shift  $\omega_D \equiv -\vec{k} \cdot \vec{v}$  and the Zeeman shift  $\omega_Z = \mu' B/\hbar$  both have opposite signs for opposite beams.

When both the Doppler and Zeeman shifts are small compared to the detuning  $\delta$ , the denominator of the force can be expanded as in Section 1.5.2 and the result becomes

$$\vec{F} = -\beta \vec{v} - \kappa \vec{r}, \quad (1.37)$$

where the damping coefficient  $\beta$  is defined in (1.34). The spring constant  $\kappa$  arises from the similar dependence of  $\vec{F}$  on the Doppler and Zeeman shifts, and is given by

$$\kappa = \frac{\mu' A}{\hbar k} \beta. \quad (1.38)$$

The force of (1.37) leads to damped harmonic motion of the atoms, where the damping rate is given by  $\Gamma_{\text{MOT}} = \beta/M$  and the oscillation frequency  $\omega_{\text{MOT}} = \sqrt{\kappa/M}$ . For magnetic field gradients  $A \approx 10$  G/cm, the oscillation frequency is typically a few kHz, and this is much smaller than the damping rate that is typically a few hundred kHz. Thus the motion is overdamped, with a characteristic restoring time to the center of the trap of  $2\Gamma_{\text{MOT}}/\omega_{\text{MOT}}^2 \approx$  several ms for typical values of the detuning and intensity of the lasers.

It is instructive to compare the optical and magnetic forces in an MOT. The optical force for an atom at rest is  $\kappa z$ , where  $\kappa$  is given in (1.38) and  $A$  is the field gradient.

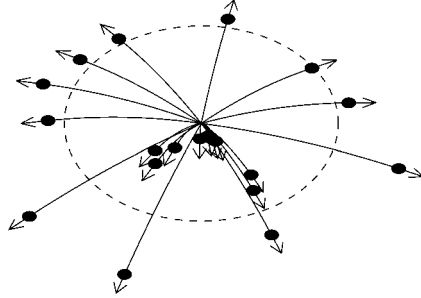


**Figure 1.19** Trajectories of the atoms after they are released from the trap. Atoms having sufficient speed will reach the edge of the laser beam, shown here schematically with the dashed circle, *before* the laser beams are switched on again and thus they are lost from the trap.

The magnetic force is simply  $\mu A$ , so their ratio is  $x \equiv F_{\text{opt}}/F_{\text{mag}} = \mu' \beta z / \mu \hbar k$ , where  $\beta$  is given in (1.34). Since  $\mu$  and  $\mu'$  do not usually differ by more than a factor of 2,  $x \sim \beta z / \hbar k \sim k z \delta / \gamma$  for typical MOT parameters ( $\delta \sim -2\gamma$ ,  $s_0 \sim 1$ ). Thus the optical force dominates the magnetic force at any distances from the MOT center that exceed a few wavelengths.

Since the MOT constants  $\beta$  and  $\kappa$  are proportional, the size of the atomic cloud can easily be deduced from the temperature of the sample. The equipartition of the energy of the system over the degrees of freedom requires that the velocity spread and the position spread are related by

$$k_B T = m v_{\text{rms}}^2 = \kappa z_{\text{rms}}^2. \quad (1.39)$$

For a temperature in the range of the Doppler temperature, the size of the MOT should be of the order of a few tenths of a mm, which is generally the case in experiments.

### 1.6.3

#### Measurements and Results

In this section we describe some of the results, which we have obtained in the laboratory in Utrecht with a standard vapor-cell MOT for Na. Here the atoms are captured from the background vapor of Na, which is produced by a small piece of Na in the cell. Since the technique does not rely on capturing atoms from a slowed beam, the setup is rather simple, which explains the popularity of the technique. Typically we capture a few million atoms and cool them to a temperature of 200  $\mu\text{K}$  at a density of  $10^{10}$  atoms/cm<sup>3</sup>. The last two numbers are very typical for an MOT, but the first number can be increased by many orders of magnitude by increasing the diameter of the laser beams, which are used to capture, cool, and trap the atoms.

Different techniques can be employed in order to measure the temperature of the atoms. Most commonly the technique of release-and-recapture is used. In this



technique, the atoms are released from the trap by shutting off the laser beam for a certain period. Since the atoms have a velocity in the trap, they will fly away ballistically, as shown in Figure 1.19. When the trapping lasers are switched on again, some of the atoms will be over the edge of the laser beam and thus will not be recaptured by the lasers. Since the atoms recaptured will fluoresce immediately after they are recaptured, the fluorescence after the laser beams are switched on again is a measure for the atoms remaining in the trap. This recapture probability as a function of the switch-off time is a direct measure of the temperature of the sample. Namely, if we neglect gravity for a moment and assume the atomic velocities have a Maxwellian distribution, the recapture probability is given by

$$P_{\text{recap}} = - \left( \frac{2}{\sqrt{\pi}} \right) \sqrt{\kappa} v_e \exp^{-\kappa v_e^2} + \text{Erf}(\sqrt{\kappa} v_e) \quad (1.40)$$

with

$$\kappa = \frac{m}{2k_B T}. \quad (1.41)$$

Here  $v_e = d/2\tau$  is the velocity that is sufficient for the atoms to travel to the edge of the laser beam with diameter  $d$  in the switch-off time  $\tau$ . In Figure 1.20, a typical measurement is shown, where the solid line is the fit of the data points to (1.40). The temperature extracted from this data set is approximately 147  $\mu\text{K}$ , but the spread between different measurements is of the order of 25  $\mu\text{K}$ , depending on the alignment of the laser beams. At these temperatures the effects of gravity are small, but if the temperature becomes smaller gravity does play a role and for very low temperatures the recapture probability no longer depends on the temperature, since the initial velocity of the atoms becomes small compared to the velocity acquired due to gravity.

To measure the spatial profile of the atoms, the fluorescence of the atoms can be imaged on a CCD camera, which makes a two-dimensional projection of the density distribution of the atoms. In Figure 1.21(a), an image of the atomic cloud is shown. Due to the large forces that act on the atoms, the alignment of the laser beams is crucial to obtain a well-balanced force of different beams and spatially filtering the laser beams helps a lot in that respect. In Figure 1.21(b), a cut through the middle of the projection is made. The spatial distribution is Gaussian and the width of the cloud in the horizontal direction is of the order of 0.29 mm. A Gaussian distribution is to be expected at low density, since the spatial spread and velocity spread are related by (1.39) and the velocity distribution is Maxwellian. However, for higher densities the density in the center of the cloud is limited due to rescattering of the fluorescent light by the atoms and the density at the center becomes constant. This leads to a flattening of the intensity in the center of the profile. Some care has to be taken when analyzing these images. When the density in the center is so large that light can no longer escape the cloud before being reabsorbed, the fluorescence is no longer a measure for the density distribution and other means to measure it have to be devised.

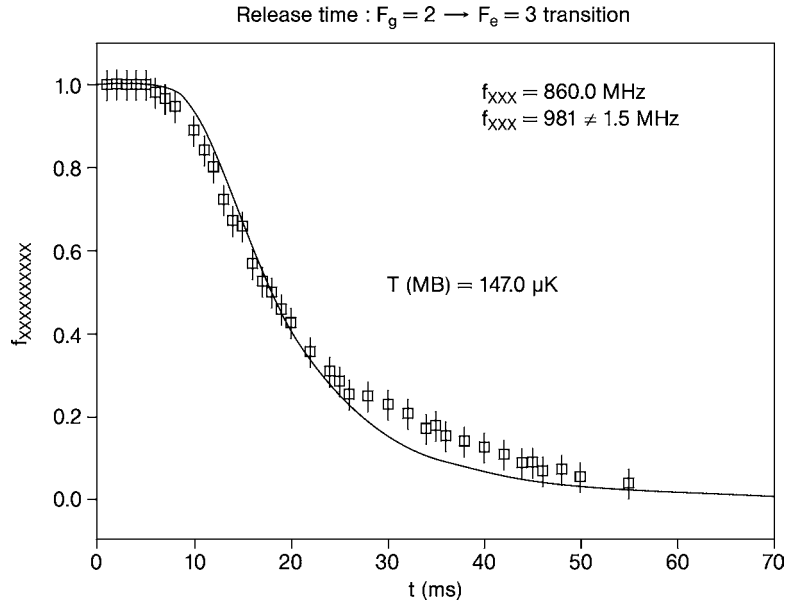


**Figure 1.20** The recapture probability  $P_{\text{recap}}$  of the atoms as a function of the shut-off time  $\tau$ . The data are shown by the squares and the fit to (1.40) is shown by the solid line.

## 1.7 Cooling Below the Doppler Limit

### 1.7.1 Introduction

In response to the surprising measurements of temperatures below  $T_D$ , two groups developed a model of laser cooling that could explain the lower temperatures [39,40]. The key feature of this model that distinguishes it from the earlier picture was the inclusion of the multiplicity of sublevels that make up an atomic state (e.g., Zeeman and hfs). The dynamics of optically pumping atoms among these sublevels provides the new mechanism for producing the ultralow temperatures [35].

The nature of this cooling process is fundamentally different from the Doppler laser cooling process discussed in the previous section. In that case, the differential absorption from the laser beams was caused by the Doppler shift of the laser frequency, and the process is therefore known as Doppler cooling. In the cooling process described in this section, the force is still caused by differential absorption of light from the two laser beams, but the velocity-dependent differential rates, and hence the cooling, relies on the nonadiabaticity of the optical pumping process. Since lower temperatures can usually be obtained with this cooling process, it is called sub-Doppler laser cooling [35, 36, 41].

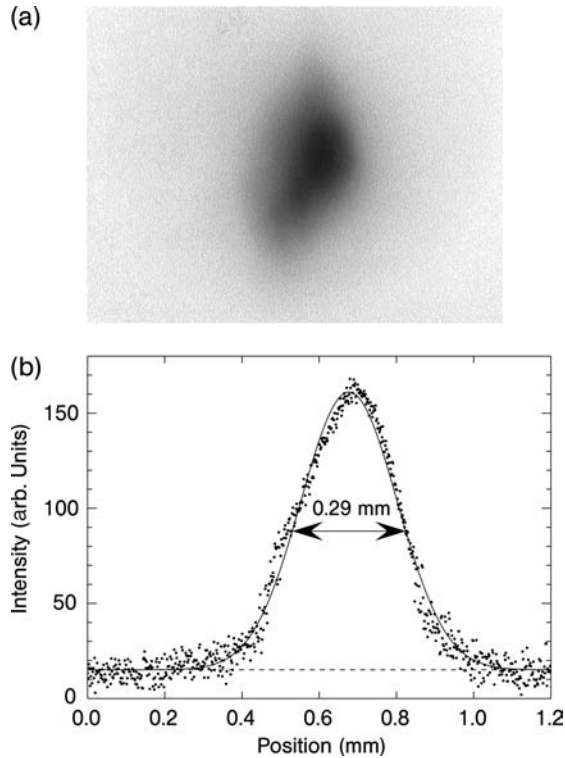


**Figure 1.21** (a) Image taken with a CCD camera of the fluorescence of a cloud of atoms in an MOT. (b) Cut of the intensity distribution through the center of the cloud. The distribution is Gaussian with a width of 0.29 mm in this case.

### 1.7.2

#### Linear $\perp$ Linear Polarization Gradient Cooling

One of the most instructive models for discussion of sub-Doppler laser cooling was introduced by Dalibard and Cohen-Tannoudji [39] and their work serves as the basis for this section. They considered the case of orthogonal linear polarization of two counterpropagating laser beams that damp atomic motion in one dimension. The polarization of this light field varies over half of a wavelength from linear at  $45^\circ$  to the polarization of the two beams, to  $\sigma^+$ , to linear but perpendicular to the first direction, to  $\sigma^-$ , and then it cycles (see Figure 1.22). To study the effects of this polarization gradient on the cooling process, they considered a  $J_g = 1/2$  to  $J_e = 3/2$  transition. This is one of the simplest transitions that shows sub-Doppler cooling.

In the place where the light field is purely  $\sigma^+$ , the pumping process drives the ground-state population to the  $M_g = +1/2$  sublevel. This optical pumping occurs because absorption always produces  $\Delta M = +1$  transitions, whereas the subsequent

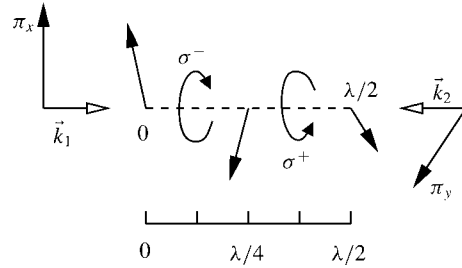


**Figure 1.22** Spatial variation of the optical electric field in the lin  $\perp$  lin configuration showing the polarization gradient used for laser cooling.

spontaneous emission produces  $\Delta M = \pm 1, 0$ . Thus the average is  $\Delta M \geq 0$  for each scattering event. For  $\sigma^-$ -light the population will be pumped toward the  $M_g = -1/2$  sublevel. Thus in traveling through a half wavelength in the light field, atoms have to readjust their population completely from  $M_g = +1/2$  to  $M_g = -1/2$  and back again.

The light shift of the atomic energy levels plays a crucial role in this scheme of sub-Doppler cooling, and the changing polarization has a strong influence on the light shifts. Since the coupling between the states depends on the magnetic quantum numbers and on the polarization of the light field, the light shifts are different for different magnetic sublevels. The ground-state light shift is negative for a laser tuning below resonance ( $\delta < 0$ ) and positive for  $\delta > 0$  (see Eq. (1.11)).

In the present case of orthogonal linear polarizations and  $J = 1/2 \rightarrow 3/2$ , the light shift for the magnetic substate  $M_g = 1/2$  is three times larger than that of the  $M_g = -1/2$  substate when the light field is completely  $\sigma^+$ . On the other hand, when the light field becomes  $\sigma^-$ , the shift of  $M_g = -1/2$  is three times larger. So in this case the optical pumping discussed above causes there to be a larger population in the state with the larger light shift. This is generally true for any transition  $J_g$  to  $J_e = J_g + 1$ . A schematic diagram showing the populations and light shifts for this particular case of negative detuning is shown in Figure 1.23.

To discuss the origin of the cooling process in this polarization gradient scheme, consider atoms with a velocity  $v$  at a position where the light is  $\sigma^+$ -polarized, as shown at the lower left of Figure 1.23. The light optically pumps such atoms to the strongly negative light-shifted  $M_g = +1/2$  state. In moving through the light field, atoms must increase their potential energy (climb a hill) because the polarization of the light is changing and the state  $M_g = 1/2$  becomes less strongly coupled to the light field. After traveling a distance  $\lambda/4$ , atoms arrive at a position where the light field is  $\sigma^-$ -polarized, and are optically pumped to  $M_g = -1/2$ , which is now lower than the  $M_g = 1/2$  state. Again the moving atoms are at the bottom of a hill and start to climb. In climbing the hills, the kinetic energy is converted to potential energy, and in the optical pumping process, the potential energy is radiated away because the spontaneous emission is at a higher frequency than the absorption (see Figure 1.23). Thus atoms seem to be always climbing hills and losing energy in the

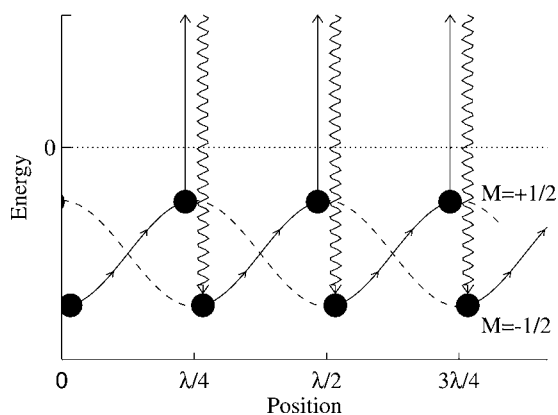


**Figure 1.23** The spatial dependence of the light shifts of the ground-state sublevels of the  $J = 1/2 \leftrightarrow 3/2$  transition for the case of the lin  $\perp$  lin polarization configuration. The arrows show the path followed by atoms being cooled in this arrangement. Atoms starting at  $z = 0$  in the  $M_g = +1/2$  sublevel must climb the potential hill as they approach the  $z = \lambda/4$  point where the light becomes  $\sigma^-$  polarized, and there they are

optically pumped to the  $M_g = -1/2$  sublevel. Then they must begin climbing another hill toward the  $z = \lambda/2$  point where the light is  $\sigma^+$  polarized and they are optically pumped back to the  $M_g = +1/2$  sublevel. The process repeats until the atomic kinetic energy is too small to climb the next hill. Each optical pumping event results in absorption of light at a lower frequency than emission, thus dissipating energy to the radiation field.

process. This process brings to mind a Greek myth, and is thus called “Sisyphus laser cooling.”

The cooling process described above is effective over a limited range of atomic velocities. The damping is maximum for atoms that undergo one optical pumping process while traveling over a distance  $\lambda/4$ . Slower atoms will not reach the hilltop before the pumping process occurs and faster atoms will already be descending the hill before being pumped toward the other sublevel. In both the cases the energy loss are smaller and therefore the cooling process less efficient.

The friction coefficient for this sub-Doppler process is larger by a factor  $(2|\delta|/\gamma)$  than the maximum friction coefficient for Doppler laser cooling. It can be shown that the momentum diffusion coefficient of this process is of the same order of magnitude as that of Doppler cooling, so that the temperature will be smaller than the Doppler temperature by the same factor (Figure 1.24). Furthermore, it shows that the friction coefficient for this case is independent of intensity, since both  $\Delta E$  and  $\gamma_p$  are proportional to the intensity.

### 1.7.3

#### Magnetically Induced Laser Cooling

Although the first models that described sub-Doppler cooling relied on the polarization gradient of the light field as above, it was soon realized that a light field of constant polarization in combination with a magnetic field could also produce

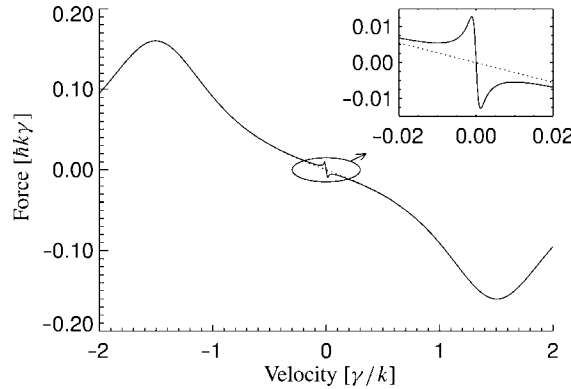


**Figure 1.24** The force as a function of velocity for atoms in a lin  $\perp$  lin polarization gradient cooling configuration with  $s_0 = 0.5$  and  $\delta = 1.5\gamma$ . The solid line is the combined force of Doppler and sub-Doppler cooling, whereas the dashed line represents the force

for Doppler cooling only. The inset shows an enlargement of the curve around  $v = 0$ . Note, the strong increase in the damping rate over a very narrow velocity range that arises from the sub-Doppler process.

sub-Doppler cooling [42]. In this process, the atoms are cooled in a standing wave of circularly polarized light.

There is a simple model using the  $J_g = 1/2$  to  $J_e = 3/2$  transition to describe this phenomenon [41]. In the absence of a magnetic field, the  $\sigma^+$  light field drives the population to the  $M_g = +1/2$  sublevel. Since the  $M_g = +1/2$  sublevel is more strongly coupled to the light field than  $M_g = -1/2$ , the light shift of this state is larger. Thus atoms traveling through this standing wave will descend and climb the same potential hills corresponding to  $M_g = 1/2$  and will experience no average force.

The situation changes if a small transverse magnetic field is applied. Optical pumping processes determine the atomic states in the antinodes of the standing wave light field where the light is strong. But in the nodes, where the intensity of the light field is zero, the small transverse magnetic field precesses the population from  $M_g = 1/2$  toward  $M_g = -1/2$ . Atoms that leave the nodes with  $M_g = -1/2$  are returned to  $M_g = +1/2$  in the antinodes by optical pumping in the  $\sigma^+$  light.

This cooling process is depicted in Figure 1.25 for negative detuning  $\delta < 0$ . Potential energy is radiated away in the optical pumping process as before, and kinetic energy is converted to potential energy when the atoms climb the hills again into the nodes. The whole process is repeated when the atoms travel through the next node of the light field. Again the cooling process is caused by a ‘‘Sisyphus’’ effect, similar to the case of lin  $\perp$  lin. Since this damping force is absent without the magnetic field, it is called magnetically induced laser cooling (MILC).

Efficient cooling by MILC depends critically on the relation between the Zeeman precession frequency  $\omega_Z$  and the optical pumping rate  $\gamma_p$  in the antinodes. It is clearly necessary that  $\gamma_p \gg \omega_Z$  in the antinodes where the light is strong. But as in any cooling process that depends on nonadiabatic processes, there is a limited

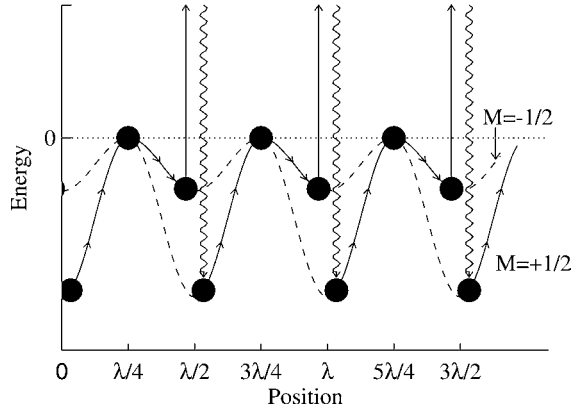


**Figure 1.25** The spatial dependence of the light shifts of the ground-state sublevels of the  $J = 1/2 \leftrightarrow 3/2$  transition for the case of a purely  $\sigma^+$  standing wave that has no polarization gradient, and is appropriate for magnetically induced laser cooling. The arrows show the path followed by atoms being cooled in this arrangement. Atoms starting at  $z = 0$  in the strongly light-shifted  $M_g = +1/2$  sublevel must climb the potential hill as they approach the node at  $z = \lambda/4$ . There they undergo Zeeman mixing in the

absence of any light and may emerge in the  $M_g = -1/2$  sublevel. They will then gain less energy as they approach the antinode at  $z = \lambda/2$  than they lost climbing into the node. Then they are optically pumped back to the  $M_g = +1/2$  sublevel in the strong light of the antinode, and the process repeats until the atomic kinetic energy is too small to climb the next hill. Each optical pumping event results in absorption of light at a lower frequency than emission, thus dissipating energy to the radiation field.

velocity range where the force is effective. For efficient cooling by MILC, the velocity cannot be too small compared to  $\omega_Z/k$  or atoms will undergo many precession cycles near the nodes and no effective cooling will result. On the other hand, if the velocity is large compared to  $\gamma_p/k$ , then atoms will pass through the antinodes in a time too short to be optically pumped to  $M_g = +1/2$  and no cooling will result either. Thus, in addition to the requirement  $\delta < 0$ , there are two other conditions on the experimental parameters that can be combined to give

$$\omega_Z < kv < \gamma_p. \quad (1.42)$$

Sub-Doppler cooling has been observed for MILC as shown in Figure 1.26 for Rb atoms cooled on the  $\lambda = 780$  nm transition in one dimension [41]. The width of the velocity distribution near  $v = 0$  is as low as 2 cm/s, much lower than the one-dimensional Doppler limit  $v_D = \sqrt{7\hbar\gamma/20M} \approx 10$  cm/s for Rb.

#### 1.7.4

##### Optical Molasses in Three Dimensions

The theoretical models and experimental results discussed so far in this section are all for the case of one dimension. The theoretical models are not easily extended to more dimensions and do not provide the same kind of analytical solutions as does 1D. One of the limitations of 3D experiments is that they are not able to

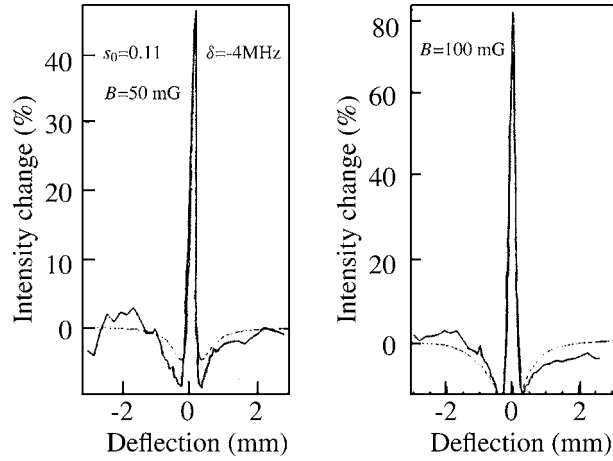


**Figure 1.26** Typical data of atomic beam collimation using circularly polarized light and a weak magnetic field on a beam of  $^{85}\text{Rb}$  atoms. The scanning hot wire was 1.3 m downstream from the interaction region. The laser parameters are defined as in Section 1.3.3 (figure from Ref. [43]).

study cooling schemes without polarization gradients, since the transverse nature of electromagnetic radiation prevents the construction of 3D radiation fields with all polarizations parallel.

One of the outcomes of the models presented in Section 1.7.2 is that the final temperature  $T_{\text{lim}}$  in polarization gradient cooling scales with the light shift  $\Delta E_g$  of the ground states, i.e.,

$$k_B T_{\text{lim}} = b \Delta E_g, \quad (1.43)$$

where  $\Delta E_g$  is the light shift of the ground state. The value of the coefficient  $b$  depends on the polarization scheme used and is 0.125 for  $\text{lin} \perp \text{lin}$  and 0.097 for  $\sigma^+ - \sigma^-$ . Note that lowering the temperature can easily be achieved by lowering the light shift, either by increasing the detuning  $\delta$  or decreasing the intensity  $s_0$ . Since this is a result of the semiclassical theory, the temperature will always be limited by the recoil temperature.

In the experiments reported by Salomon et al. [44], the temperature was measured in a 3D molasses under various configurations of the polarization. All beams were linearly polarized, but in one configuration the polarization of two counterpropagating beams was chosen to be parallel to one another and in another configuration they were chosen to be perpendicular. Results of their measurements are shown in Figure 1.27(a), where the measured temperature is plotted for different detunings as a function of the intensity. For each detuning, the data lie on a straight line through the origin. The lowest temperature obtained is  $3 \mu\text{K}$ , which is a factor 40 below the Doppler temperature and a factor 15 above the recoil temperature of Cs. If the temperature is plotted as a function of the light shift (see Figure 1.27(b)), all the data are on a single universal straight line. The slope of the line is 0.45 for the



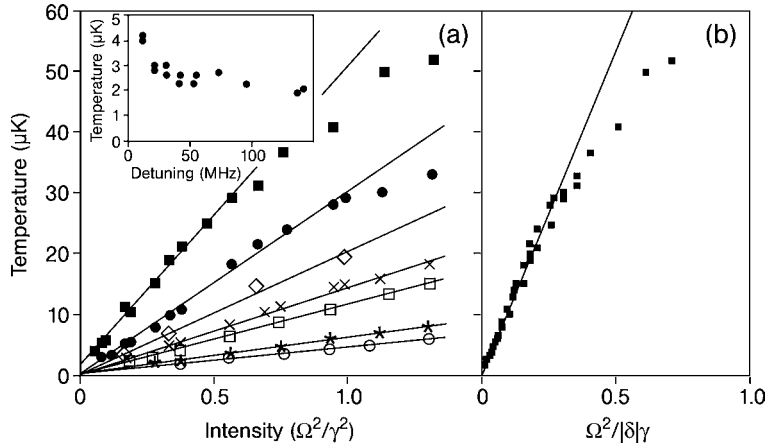


**Figure 1.27** Temperature as a function of laser intensity and detuning for Cs atoms in an optical molasses from Ref. [44]. (a) Temperature as a function of detuning for various intensities. (b) Temperature as a function of the light shift. All the data points are on a universal straight line.

parallel configuration and 0.35 for the perpendicular configuration. Both slopes are a factor of about 3 higher than the theoretical estimates of 1D and the authors ascribe this discrepancy to the three-fold increase of the number of laser beams.

## 1.8 Magnetic Trapping

The low temperatures and high densities required for BEC are not compatible with the recoil heating associated with ordinary laser cooling and optical trapping, and so different cooling and trapping mechanisms must be brought to bear on the final stages of approach to BEC. Section 1.9 describes the evaporative cooling process that is most commonly used in the final stages, and this section describes magnetic trapping that works in the dark.

The magnetic field causes a Zeeman shift  $\Delta E_Z$  of the energies of the atomic states by

$$\Delta E_Z = -\vec{\mu} \cdot \vec{B}, \quad (1.44)$$

where  $\vec{\mu}$  is the atomic magnetic moment. Since a local maximum of the magnetic field cannot be created in free space [45], atoms can only be trapped in magnetic field minima and thus can only be trapped in states that are “low field seeking,” i.e., states that shift upward with increasing field. In magnetic fields that are readily produced in the laboratory (0.1 T), typical trap depths are  $\sim 1$  K. Note that these same energy level shifts occur in the MOT, but that the force on the atoms in the MOT is predominantly from differential light scattering. As shown in Section 1.6.2,

this magneto-optical force dominates the purely magnetic force a few wavelengths away from the center of the trap.

For small magnetic fields, the projection  $M_F$  of the total angular momentum  $F$  is a good quantum number and the Zeeman shift is linear and given by

$$\Delta E_Z = g_F M_F \mu_B B, \quad (1.45)$$

where  $\mu_B = e\hbar/2m_e c$  is the Bohr magneton and  $g_F$  is the Landé factor, which is given by Eq. (4.4) of Ref. [3]. For larger magnetic field values where the Zeeman shifts become comparable to the atomic hyperfine splitting, the states from different hyperfine states start to repel one another and the shifts become more complicated. The Zeeman structure of the ground state of Na is shown in Figure 1.28. The state with  $M_F = 2$  connected to the upper hyperfine state is the easiest to trap since it has the largest shift of  $\Delta E_Z = \mu_B B$ . However, for small fields the  $M_F = -1$  state of the lower hyperfine state can also be trapped, although the energy shift  $\Delta E_Z = \mu_B B/2$  is smaller than the shift for upper hyperfine state and the maximum magnetic field for trapping is limited. This state has the advantage that collisions of atoms in the trap at very low temperatures cannot lead to inelastic losses and thus heating of the gas, since the atoms are already in the lowest energy state.

In Ref. [46] different configurations for magnetic trapping are discussed and a few of them are shown in Figure 1.29. The simplest configuration is the quadrupole configuration that is also employed for the MOT. Magnetic field contours for this trap are shown in Figure 1.30(a). When the coils are separated by 1.25 times their radius, the gradient in the radial direction is twice the gradient in the axial direction. In the case of a hexapole trap (see Figure 1.29(b)) the gradient in the center of the trap is strongly reduced (see Figure 1.30(b)), which is not very advantageous if evaporative cooling is used. Furthermore, the optical access to the atoms is inhibited by the coil on the axis.

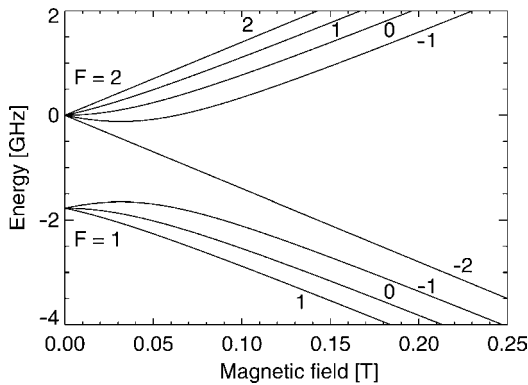


**Figure 1.28** Zeeman shifts of the ground state of Na, where the states are labeled with the projection of the total angular momentum  $F$  on the magnetic field axis. At small magnetic fields the shift are linear,

but in the range where the Zeeman shifts become comparable to the hyperfine splitting, the states start to repel each other and a more complicated pattern arises.

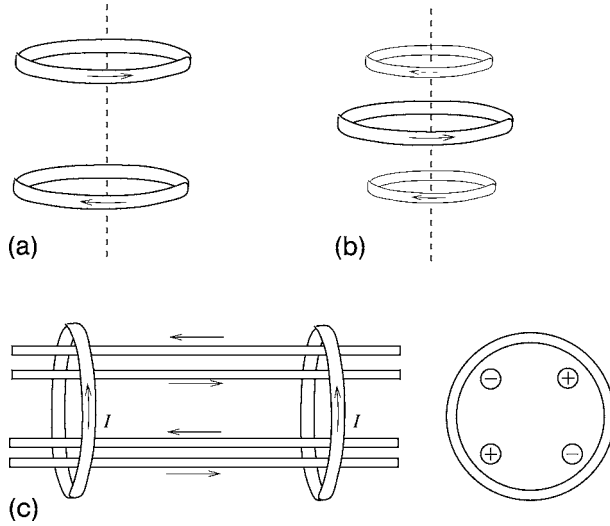


**Figure 1.29** Different magnetic field configurations to trap cold atoms with the magnetic field (adapted from Ref. [46]).

Another type of trap is the Ioffe trap, which is shown in Figure 1.29(c). The radial confinement is provided by the four bars, whereas the confinement in the axial direction is produced by the two pinch coils. In Figure 1.31 the magnetic field contours for this type of trap are shown in two different symmetry planes of the trap. The confinement in the radial direction is much stronger than in the axial direction, which allows the creation of samples with a strong asymmetry.

The advantage of the Ioffe trap over the quadrupole configuration is that the field on the axis is nonzero. Since slow atoms will always follow the magnetic field adiabatically, atoms in the center of the quadrupole trap can make a Majorana transition to the nontrapping state if the field in the center is zero. Therefore new designs for the quadrupole fields have been utilized, such as the cloverleaf [47] and QUIC trap [48], where additional coils lift the field in the center of the trap.

For the two-coil quadrupole magnetic trap of Figure 1.29(a), stable circular orbits of radius  $\rho$  in the  $z = 0$  plane can be found classically by setting  $\mu \nabla B = Mv^2/\rho$ , so  $v = \sqrt{\rho a}$ , where  $a \equiv \mu \nabla B/M$  is the centripetal acceleration supplied by the field gradient. In order for the trap to work, the atomic magnetic moments must be preserved while the atoms move around in the trap even though the trap fields change directions in a very complicated way. The condition for adiabatic motion can be written as  $\omega_Z \gg |dB/dt|/B$ , where  $\omega_Z = \mu B/\hbar$  is the Larmor precession rate in the field. The orbital frequency for circular motion is  $\omega_T = v/\rho$ , and since  $v/\rho = |dB/dt|/B$  for a uniform field gradient, the adiabaticity condition is

$$\omega_Z \gg \omega_T. \quad (1.46)$$

For the two-coil quadrupole trap, the adiabaticity condition can be easily calculated. The adiabatic condition for a practical trap ( $A \sim 1$  T/m) requires

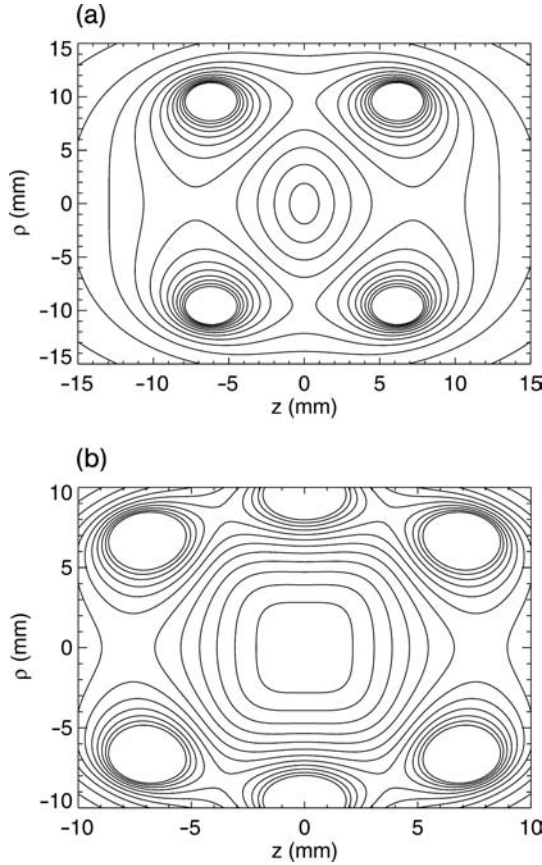


**Figure 1.30** Magnetic field contours for the quadrupole trap and the spherical hexapole trap. The current through all the coils is 100 A, the distance between the rings is 2 cm and the contours are plotted 10 G (adapted from Ref. [46]).

$\rho \gg (\hbar^2/M^2 a)^{1/3} \sim 1 \text{ } \mu\text{m}$  as well as  $v \gg (\hbar a/M)^{1/3} \sim 1 \text{ cm/s}$ . Since the non-adiabatic region of the trap is so small (less than  $10^{-18} \text{ m}^3$  compared with typical sizes of  $\sim 2 \text{ cm}$  corresponding to  $10^{-5} \text{ m}^3$ ), nearly all the orbits of most atoms are restricted to regions where they are adiabatic. Therefore, most of such laser-cooled atoms stay trapped for many thousands of orbits corresponding to several minutes. However, evaporative cooling (see Section 1.9) reduces the average total energy of a trapped sample sufficiently that the orbits are confined to regions near the origin so such losses dominate, and several schemes have been developed to prevent such losses from nonadiabatic transitions.

There have been different solutions to this problem. In the JILA-experiment the hole was rotated by rotating the magnetic field and thus the atoms do not spend sufficient time in the hole to make a spin flip. In the MIT experiment the hole was plugged by using a focused laser beam that expelled the atoms from the center of

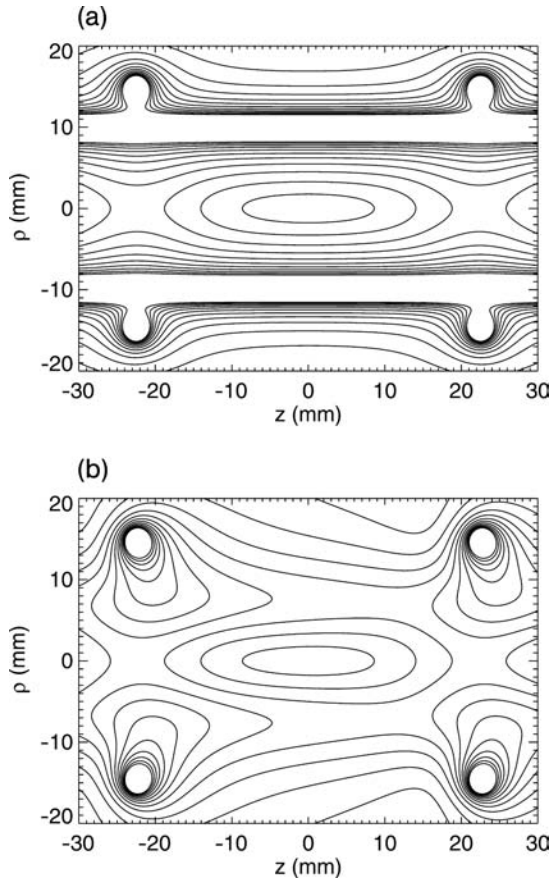


**Figure 1.31** Magnetic field contours for the Ioffe trap in the plane of the wires (a) and in the plane midway between the wires. The current through the wires is 100 A, the distance between the wires is 2 cm, the coils have a radius of 1.5 cm and the distance between the coils is 4.5 cm. The contours for the magnetic field are plotted every 10 G (adapted from Ref. [46]).

the magnetic trap. In the Rice experiment the atoms were trapped in a Ioffe trap that has a nonzero field minimum.

## 1.9 Evaporative Cooling

### 1.9.1 Introduction

Laser cooling leads to the production of samples of atoms with low temperature and high density. In the 1920s Bose and Einstein predicted that for sufficiently low

temperature and high density, a gas of atoms undergoes a phase transition that is now called Bose–Einstein condensation (BEC). This phase transition is predicted to occur at a phase-space density  $\rho \equiv n\lambda_{\text{deB}}^3 \cong 2.612$ , where  $n$  is the density of the gas and  $\lambda_{\text{deB}} = h/M\bar{v} = h/\sqrt{3Mk_{\text{B}}T}$  is the deBroglie wavelength of the atoms. For ordinary gases at room temperature and pressure,  $\rho \sim 10^{-6}$ , but in a practical atomic beam oven,  $\rho \sim 3 \times 10^{-10}$ .

Achieving BEC has been one of the holy grails in physics for many years, and from the beginning of laser cooling it was clear that this could be one of the possible routes for achieving it. With laser cooling one can obtain  $\mu\text{K}$  temperatures with small loss of atoms so that the phase-space density can be increased. However, in the mid-1990s it became clear that the increase in phase-space density by laser cooling of alkali atoms had reached its limit. If the density of the sample becomes too large, light scattered by one atom is reabsorbed by others, causing a repulsion between them. For resonant light, the optical thickness of a sample of atoms that has been laser cooled to the recoil limit and compressed to  $\rho \sim 1$  is only one optical wavelength, so light can neither enter nor escape a reasonably sized sample.

The increase of density also leads to an increase in the collision rate. The collision rate between atoms with one in the excited state (S+P collisions) is also much larger at low temperatures than the rate for such collisions with both atoms in the ground state (S+S collisions). Since S+P collisions are generally inelastic, and since the inelastic energy exchange generally leads to heating of the atoms, increasing the density increases the loss of cold atoms. To achieve BEC, resonant light should therefore be avoided, and thus laser cooling alone is not the most likely route for achieving BEC.

A more promising route to BEC is the technique of evaporative cooling. This method is based on the preferential removal of those atoms from a confined sample with an energy higher than the average energy, followed by a rethermalization of the remaining gas by elastic collisions. Although evaporation is a process that occurs in nature, it was applied to atom cooling for the first time in 1988 [49]. One way to think about evaporative cooling is to consider cooling of a cup of coffee. Since the most energetic molecules evaporate from the coffee and leave the cup, the remaining atoms obtain a lower temperature and are cooled. Furthermore, it requires the evaporation of only a small fraction of the coffee to cool it by a considerable amount. Thus even though the method results in the removal of some of the atoms in a trap, those that remain have much lower average energy (temperature) and so they occupy a smaller volume near the bottom of the trap, thereby increasing their density. Since both the temperature and the volume decrease, the phase-space density increases.

This section describes a model of evaporative cooling. Since such cooling is not achieved for single atoms but for the whole ensemble, an atomic description of the cooling process must be replaced by thermodynamic methods. These methods are completely different from the rest of the material in the chapter, and will therefore remain rather elementary.

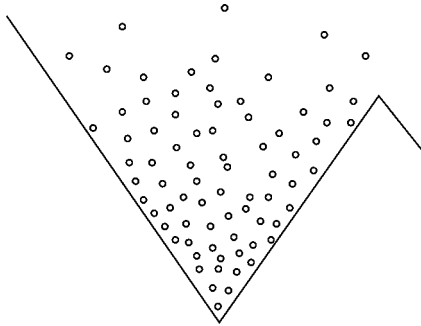


**Figure 1.32** Principle of the evaporation technique. Once the trap depth is lowered, atoms with energy above the trap depth can escape and the remaining atoms reach a lower temperature.

### 1.9.2

#### Basic Assumptions

Evaporative cooling works by the preferential removal of atoms having an energy higher than the average energy, as suggested schematically in Figure 1.32. If the atoms are trapped, it can be achieved by lowering the depth of the trap, thereby allowing the atoms with energies higher than the trap depth to escape, as discussed first by Hess [50]. Elastic collisions in the trap then lead to a rethermalization of the gas. To sustain the cooling process the trap depth can be lowered continuously, achieving a continuous decrease of the temperature. Such a process is called forced evaporation. Although more refined techniques have been developed, this technique was first employed for evaporative cooling of hydrogen [49, 51–53].

Several models have been developed for this process, but the simplest one was developed by Davis et al. [54], and is mainly of pedagogical value [55]. In this model the trap depth is lowered in one single step and the effect on the thermodynamic quantities, such as temperature, density, and volume, is calculated. Although the process can be repeated and the effects of multiple steps added up cumulatively, forced evaporative cooling is a continuous process and should be described by other models. However, the results of the simple model provide considerable insight to the process without resorting to tedious calculations.

In many models of evaporative cooling the following assumptions are made:

1. The gas behaves sufficiently ergodically, i.e., the distribution of atoms in phase space (both position and momentum) depends only on the energy of the atoms and the nature of the trap.
2. The gas is described by classical statistics and is assumed to be far from the transition point to the BEC phase ( $\rho \ll 1$ ).
3. The quantum mechanical scattering is pure s-wave, i.e., the temperature is sufficiently low that all higher partial waves do not contribute to the cross section. Furthermore, the cross section for elastic scattering is energy-independent and

is given by  $\sigma = 8\pi a^2$ , where  $a$  is the scattering length. Also, it is assumed that the ratio of elastic to inelastic collision rates is sufficiently large that the elastic collisions dominate.

4. Evaporation preserves the thermal nature of the distribution, i.e., the thermalization is much faster than the rate of cooling.
5. Atoms that escape from the trap neither collide with the remaining atoms nor exchange energy with them. This is called full evaporation.

The simple model uses all of these assumptions, and their implications will be discussed later in the section.

### 1.9.3

#### The Simple Model

The first step in applying this simple model is to characterize the trap by calculating how the volume of a trapped sample of atoms changes with temperature  $T$ . Consider a trapping potential that can be expressed as a power law given by

$$U(x, y, z) = \epsilon_1 \left| \frac{x}{a_1} \right|^{s_1} + \epsilon_2 \left| \frac{y}{a_2} \right|^{s_2} + \epsilon_3 \left| \frac{z}{a_3} \right|^{s_3}, \quad (1.47)$$

where  $a_j$  is a characteristic length and  $s_j$  the power for a certain direction  $j$ . Then one can prove [56] that the volume occupied by trapped atoms scales as  $V \propto T^\xi$ , where

$$\xi \equiv \frac{1}{s_1} + \frac{1}{s_2} + \frac{1}{s_3}. \quad (1.48)$$

Thus the effect of the potential on the volume of the trapped sample for a given temperature can be reduced to a single parameter  $\xi$ . This parameter is independent of how the occupied volume is defined, since many different definitions lead to the same scaling. When a gas is held in a 3D box with infinitely high walls, then  $s_1 = s_2 = s_3 = \infty$  and  $\xi = 0$ , which means that  $V$  is independent of  $T$ , as expected. For a harmonic potential in 3D,  $\xi = 3/2$ , for a linear potential in 2D  $\xi = 2$ , and for a linear potential in 3D,  $\xi = 3$ .

The evaporative cooling model itself [54] starts with a sample of  $N$  atoms having a temperature  $T$  held in an infinitely deep trap. The strategy for using the model is to choose a finite quantity  $\eta$ , and then (1) lower the trap depth to a value  $\eta k_B T$ , (2) allow for a thermalization of the sample by collisions, and (3) determine the change in phase-space density  $\rho$ .

Only two parameters are needed to completely determine all the thermodynamic quantities for this process (the values after the process are denoted by a prime). One of these is  $\nu \equiv N'/N$ , the fraction of atoms remaining in the trap after the cooling. The other<sup>2)</sup> is  $\gamma$ , a measure of the decrease in temperature caused by the release of hot atoms and subsequent cooling, modified by  $\nu$ , and defined as

2) This  $\gamma$  is not to be confused with the natural width of the excited state.



$$\gamma \equiv \frac{\log(T'/T)}{\log(N'/N)} = \frac{\log(T'/T)}{\log \nu}. \quad (1.49)$$

This yields a power-law dependence for the decrease of the temperature caused by the loss of the evaporated particles, namely,  $T' = T\nu^\gamma$ . The dependence of the other thermodynamic quantities on the parameters  $\nu$  and  $\gamma$  can then be calculated.

The scaling of  $N' = N\nu$ ,  $T' = T\nu^\gamma$ , and  $V' = V\nu^{\gamma\xi}$  can provide the scaling of all the other thermodynamic quantities of interest by using the definitions for the density  $n = N/V$ , the phase-space density  $\rho = n\lambda_{\text{deB}}^3 \propto nT^{-3/2}$ , and the elastic collision rate  $k_{\text{el}} \equiv n\sigma v \propto nT^{1/2}$ . The results are given in Table 1.5. For a given value of  $\eta$ , the scaling of all quantities depends only on  $\gamma$ . Note that for successive steps  $j$ ,  $\nu$  has to be replaced with  $\nu^j$ .

In order to determine the change of the temperature in the cooling process, it is necessary to consider in detail the distribution of the atoms in the trap. The density of states for an ideal gas in free space is given by [7]

$$D(E) = \frac{2\pi(2M)^{3/2}VE^{1/2}}{h^3}. \quad (1.50)$$

However, for atoms in a trap the density of states is affected by the trapping potential  $U(x, y, z)$  and becomes [56]

$$D(E) = \frac{2\pi(2M)^{3/2}}{h^3} \int_V \sqrt{E - U(x, y, z)} d^3r. \quad (1.51)$$

The fraction of atoms remaining in the trap after decreasing the trap depth to  $\eta k_B T$  becomes

$$\nu = \frac{1}{N} \int_0^{\eta k_B T} D(E) e^{-(E-\mu)/k_B T} dE, \quad (1.52)$$

where the exponential factor stems from the Maxwell–Boltzmann distribution of the atoms, and  $\mu$  is the chemical potential. For  $\eta = \infty$ ,  $\nu = 1$  and this determines the chemical potential  $\mu$  for  $N$  atoms [56]. Substituting this relation for  $\mu$  into (1.52) yields

$$\nu = \int_0^\eta \Delta(\epsilon) e^{-\epsilon} d\epsilon, \quad (1.53)$$

**Table 1.5** Exponent  $q$  for the scaling of the thermodynamic quantities  $X' = X\nu^q$  with the reduction  $\nu$  of the number of atoms in the trap.

Thermodynamic variable	Symbol	Exponent $q$
Number of atoms	$N$	1
Temperature	$T$	$\gamma$
Volume	$V$	$\gamma\xi$
Density	$n$	$1 - \gamma\xi$
Phase-space density	$\rho$	$1 - \gamma(\xi + 3/2)$
Collision rate	$k$	$1 - \gamma(\xi - 1/2)$

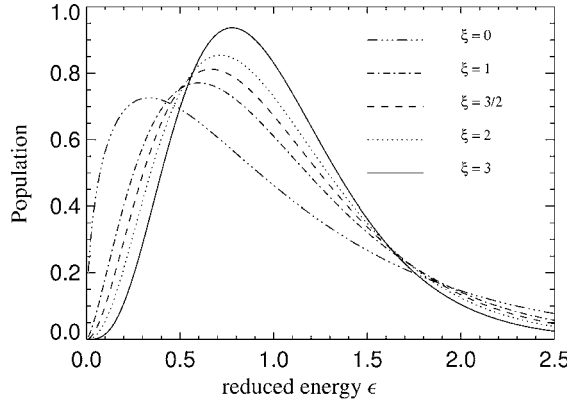


**Figure 1.33** Reduced density of states  $\Delta(\epsilon)$  as a function of the scaled energy  $\tilde{\epsilon} = \epsilon/(\xi + 3/2)$  for various trapping potentials, indicated by their parameter  $\xi$ .

where the reduced energy is defined as  $\epsilon \equiv E/k_B T$ . Furthermore, the reduced density of states  $\Delta(\epsilon)$  is given by

$$\Delta(\epsilon) \equiv \frac{\epsilon^{\xi+1/2}}{\Gamma(\xi + 3/2)}, \quad (1.54)$$

with  $\Gamma(x)$  the complete gamma function. Figure 1.33 shows the reduced density of states as a function of  $\tilde{\epsilon} = \epsilon/(\xi + 3/2)$  for various values of  $\xi$ . The scaling of  $\epsilon$  is performed so that the reduced density of states is nearly independent of  $\xi$ . The results for different potentials can therefore be compared directly.

The integral in (1.53) can be written in terms of the incomplete gamma function  $\Gamma_{\text{inc}}$  to give

$$\nu = \frac{\Gamma_{\text{inc}}(\xi + 3/2, \eta)}{\Gamma(\xi + 3/2)}. \quad (1.55)$$

Note that the fraction of atoms remaining is fully determined by the final trap depth  $\eta$  for given potential characterized by the trap parameter  $\xi$ .

The averaged reduced energy  $\bar{\epsilon}$  of the atoms before truncation is given by

$$\bar{\epsilon} = \frac{\int_0^\infty \epsilon \Delta(\epsilon) e^{-\epsilon} d\epsilon}{\int_0^\infty \Delta(\epsilon) e^{-\epsilon} d\epsilon} = \frac{\Gamma(\xi + 5/2)}{\Gamma(\xi + 3/2)} = \xi + 3/2. \quad (1.56)$$

The average energy  $\bar{\epsilon}'$  after truncation is given by the same expression, when the upper boundary is changed from  $\infty$  to  $\eta$ . The average energy is thus

$$\bar{\epsilon}' = \frac{\Gamma_{\text{inc}}(\xi + 5/2, \eta)}{\Gamma_{\text{inc}}(\xi + 3/2, \eta)}. \quad (1.57)$$

Since the average energy is directly proportional to the temperature, the ratio  $T'/T$  is given by

$$\frac{T'}{T} = \frac{\bar{\epsilon}'}{\bar{\epsilon}} = \nu^\gamma, \quad (1.58)$$

or

$$\gamma = \frac{\log(T'/T)}{\log(N'/N)} = \frac{\log(\bar{\epsilon}'/\bar{\epsilon})}{\log \nu}. \quad (1.59)$$

For each evaporated atom the energy carried away  $\epsilon_{\text{out}}$  is given by

$$\epsilon_{\text{out}} = \frac{\bar{\epsilon} - \bar{\epsilon}'}{1 - \nu} = (\xi + 3/2) \frac{1 - \nu^{\gamma+1}}{1 - \nu}. \quad (1.60)$$

For large  $\eta$ , the value of  $\nu$  approaches 1 so the denominator  $(1 - \nu)$  can be treated as small. Then

$$\gamma = \frac{\epsilon_{\text{out}}}{\xi + 3/2} - 1. \quad (1.61)$$

so in that case,  $\gamma$  is just the excess energy above the average energy, which is carried away by the evaporated atoms.

The results of the model are given in Figure 1.34. Apart from the 3D box potential ( $\xi = 0$ ) the results for the number of atoms and the temperature are nearly identical for different potentials. However, for a stronger potential (larger  $\xi$ ) the decrease in the volume with decreasing temperature is much larger and therefore the increase in density  $n$  is much larger. Not only does this lead to a larger increase in phase-space density  $\rho$ , but this is also important for the rethermalization of the atoms. As the results show, the elastic collision rate also increases strongly for a stronger potential. This way the rethermalization speeds up considerably and the cooling process can be accelerated. In the case of a weak potential ( $\xi$  between 0 and 1) the collision rate decreases for all values of  $\eta$  and therefore the cooling process eventually stops. Thus the model indicates that BEC cannot be obtained in such potentials.

#### 1.9.4

##### Speed and Limits of Evaporative Cooling

So far the speed of the evaporative cooling process has not been considered. As an extreme example, consider the case of an extremely large value of  $\eta$  where one just has to wait for a single event where one particle has all the energy of the system. Evaporation of that single particle then cools the whole system to zero temperature [55]. More realistically one can consider the following two cases. If the trap depth is ramped down too quickly, the thermalization process does not have time to run its course and the process becomes less efficient. On the other hand, if the trap depth is ramped down too slowly, the loss of particles by inelastic collisions becomes important, thereby making the evaporation inefficient.

The speed of the evaporation can be found from the principle of detailed balance [55]. It states that elastic collisions produce atoms with energy larger than  $\eta k_B T$  at a rate that is given by the number of atoms with energy larger than this divided by their collision time. The velocity of atoms with this energy is given by  $v = \sqrt{2\eta k_B T/M} = \bar{v} \sqrt{3\eta/2}$ , where  $\bar{v}$  is the average velocity for given temperature. The fraction of atoms in the MB-distribution with  $\epsilon > \eta$  for large  $\eta$  is given by

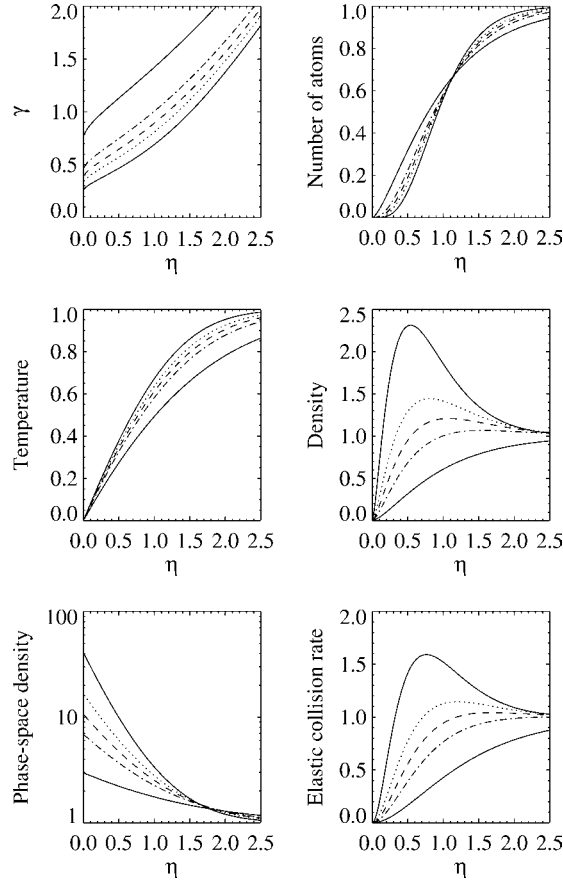


**Figure 1.34** Result of the model for evaporation for different values of  $\xi$  (see Figure 1.33) for the thermodynamic quantities: (1)  $\gamma$ , (2) number of atoms, (3) temperature, (4) density, (5) phase-space density, and (6) elastic collision rate (figure adapted from Ref. [54]).

$$f(\epsilon > \eta) = e^{-\eta} \sqrt{3\eta/2}. \quad (1.62)$$

The elastic collision rate is given by  $k_{\text{el}} = n\sigma v$ . The rate of evaporated atoms  $dN/dt$  becomes

$$\frac{dN}{dt} = -Nf(\epsilon > \eta)k_{\text{el}} = -n\sigma\bar{v}\eta e^{-\eta}N \equiv -\Gamma_{\text{ev}}N. \quad (1.63)$$

The average elastic scattering rate depends on the relative velocity and not on the average velocity of the atoms. Thus the average of  $k_{\text{el}}$  is  $\bar{k}_{\text{el}} = 4n\sigma\bar{v}/\sqrt{3\pi}$ . The ratio of the evaporation time and the elastic collision time then becomes

$$\frac{\tau_{\text{ev}}}{\tau_{\text{el}}} = \frac{\sqrt{2}e^{\eta}}{\eta}. \quad (1.64)$$

Note that this ratio increases exponentially with  $\eta$ .

For the evaporation of the atoms, it is important that atoms with an energy above the cut-off are expelled from the trap. By lowering the depth of the trap on one side, atoms can only escape in one dimension, but by using rf-evaporation, one can expel the atoms in all three dimensions equally and thus obtain a true 3D evaporation. However, in the case of the TOP-trap, even rf evaporation takes place in 2D because the atoms are evaporated along the outer side of the cloud that is exposed to the highest magnetic field on the average. This is a cylinder along the direction of rotation axis of the magnetic field and thus is only 2D.

Once the average energy of the atoms becomes very small, the atoms sag in the magnetic field due to gravity and the outer side of the cloud is no longer at a constant magnetic field. Atoms at the bottom of the trap experience the highest magnetic field and thus the evaporation becomes 1D. In case of harmonic confinement,  $U_{\text{trap}} = U''z^2/2$ , atoms with an energy of  $\eta k_B T$  make excursions of the order of

$$z \approx \sqrt{2\eta k_B T / U''}. \quad (1.65)$$

Now the gravitational energy is given by  $U_{\text{grav}} = mgz$  and when this energy becomes comparable to total energy, 3D evaporation stops and the evaporation becomes 1D. Thus the limiting temperature for 1D evaporation to take place is given by [55]

$$k_B T < \frac{2\eta(mg)^2}{\mu B''}. \quad (1.66)$$

For a value of a curvature of  $B'' = 500 \text{ G/cm}^2$  the limiting temperature becomes  $1 \mu\text{K}$  for  ${}^7\text{Li}$ ,  $10 \mu\text{K}$  for  ${}^{23}\text{Na}$ , and  $150 \mu\text{K}$  for  ${}^{87}\text{Rb}$ . Beyond this temperature evaporation becomes less efficient.

In the three experiments that obtained BEC for the first time in 1995, this problem of “gravitational sag” was not known but its presence did not prevent the experimentalists from observing BEC. The experiments succeeded for different reasons: the light mass ( ${}^7\text{Li}$ ), tight confinement ( ${}^{23}\text{Na}$ ), and TOP trap ( ${}^{87}\text{Rb}$ ). It is another violation of Murphy’s law that the solutions in these experiments were found without really knowing the problem [55].

### 1.9.5

#### Experimental Results

In all the earliest experiments that achieved BEC, the evaporative cooling was “forced” by inducing rf transitions to magnetic sublevels that are not bound in the magnetic trap. Atoms with the highest energies can access regions of the trap where the magnetic field is stronger, and thus their Zeeman shifts would be larger. A correspondingly high-frequency rf field would cause only these most energetic atoms to undergo transitions to states that are not trapped, and in so doing, the departing atoms carry away more than the average energy. Thus a slow sweep of

Table 1.6 Results obtained with evaporative cooling for the achievement of BEC [55].<sup>a</sup>

Group	Atom	$N$ ( $10^6$ )	$n$ ( $10^{12} \text{ cm}^{-3}$ )	$T$ ( $\mu\text{K}$ )	$\rho$ ( $10^{-6}$ )	$\eta_{\text{tot}}$
Rice	$^7\text{Li}$	200	0.07	200	7	1.7
		0.1	1.4	0.4		
MIT	$^{23}\text{Na}$	1000	0.1	200	2	1.9
		0.7	150	2		
JILA	$^{87}\text{Rb}$	4	0.04	90	0.3	3.0
		0.02	3	0.17		

<sup>a</sup>The first line represents the starting point in each case, and the second line the end point.

the rf frequency from high to low would continuously shave off the high-energy tail of the energy distribution, and thereby continuously drive the temperature lower and the phase-space density higher.

In Table 1.6 the results of evaporative cooling from the first three groups that have obtained BEC are given. The success of evaporative cooling using this rf-shaving technique demonstrates that it is much easier to select high-energy atoms and waste them than to cool them.

### 1.10 Beyond Optical Molasses

Although evaporative is a very powerful technique to obtain BEC, at least for the final phase of the cooling process, the quest for obtaining BEC in an all optical way remained open. One advantage of obtaining BEC in an all optical way is the fact that in the cooling process the number of atoms remains constant. Using evaporation, one loses orders of magnitude of atoms in the cooling process (see Table 1.6). There have been two ways to obtain an all optical BEC. One way is to cool atoms in an optical lattice and another way is to cool atoms held in an optical trap using a  $\text{CO}_2$  laser.

#### 1.10.1 Raman Sideband Cooling

Raman sideband cooling of atoms in an optical lattice is very reminiscent of the same cooling process introduced for ions. In an optical lattice atoms are bound in optical traps with dimensions of  $\lambda/2$ , where  $\lambda$  is the optical wavelength. If the trapping potential is sufficiently deep, the atomic energy is restricted to narrow bands in the harmonic optical potential. By careful choice of the laser parameters, atoms can be pumped toward the lowest vibrational state and thus cooled.

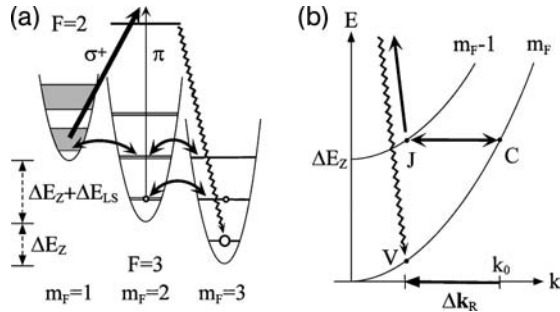


**Figure 1.35** Atoms in different magnetic substates are coupled by Raman transitions, which are resonant due to a Zeeman shift of the magnetic substates. By optical pumping atoms can be pumped back to the lowest state, thus making the cooling cycle complete [58].

To utilize the band structure a method was proposed by Hamann et al. [57]. Here we will describe the 3D-version of the same scheme by Kerman et al. [58], which is shown schematically in Figure 1.35. A far detuned optical lattice is used to trap the atoms in different  $M_F$  states. A small magnetic field shifts different  $M_F$  states with respect of each other and by introducing a small angle between the magnetic field axis and the optical lattice, the light of the optical lattice induces Raman transitions between different  $M_F$  states. By using the appropriate magnetic field, the vibrational state  $n$  of magnetic substate  $M_F = 3$  can be made resonant with state  $n - 1$  of  $M_F = 2$  or  $n - 2$  of  $M_F = 1$ . In the Raman process the atoms loses one or two quanta of vibrational energy. If the atom in state  $M_F = 1$  is optically pumped to the excited state by an additional  $\sigma^+$  laser beam and subsequently decays to the  $M_F = 3$  state by spontaneous emission, the vibrational quantum number is conserved in the Lamb–Dicke regime. Thus the atoms loses in this process (2 Raman transitions followed by absorption and spontaneous emission) 2 quanta of vibrational energy. Since the process can be repeated, the atoms can be cooled to the lowest vibrational state and spin polarized in the same time. Note that by choosing the optical pumping beam resonant from the  $F = 3$  ground state to the  $F = 2$  upper state, atoms in the  $M_F = 3$  ground state cannot be optically pumped and thus are decoupled in the lowest vibrational state from the light. To depopulate the lowest state of the  $M_F = 2$  ground state, a small  $\pi$  component is added to the optical pumping beam.

This cooling in an optical lattice has two advantages over cooling of free atoms in an optical molasses. Firstly, atoms are isolated in the optical lattice from each other and thus cannot undergo inelastic collisions, which heat the atoms. Secondly, since the reabsorption of spontaneously emitted photon by the other atoms is strongly reduced, the heating of the atoms in this process is reduced [59]. In Figure 1.36 it is shown that the heating of the atoms of  $8 \text{ nK}/10^{10} \text{ atoms/cm}^3$  is strongly reduced due to the optical lattice compared to  $600 \text{ nK}/10^{10} \text{ atoms/cm}^3$  for optical molasses. This way phase-space densities have been obtained for Cs of  $1/500$ , which is 3

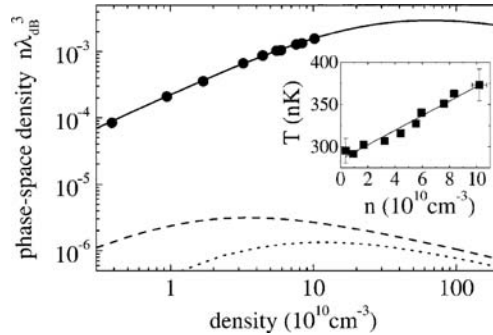


**Figure 1.36** Phase-space density  $\rho$  as a function of the density  $n$  for Raman sideband cooling. Circles indicated data points and solid line is a fit to the data with a heating rate of  $8 \text{ nK}/10^{10} \text{ atoms/cm}^3$ . For comparison, dotted line indicates the results for optical molasses, whereas dashed line indicate the result for “gray” optical molasses [58].

orders of magnitude larger compared to ordinary optical molasses, but still 2 orders of magnitude away from quantum degeneracy. A pulsed version of this scheme as implemented by Han et al. [60] yielded a phase-space density of  $1/30$ , still short of quantum degeneracy.

### 1.10.2

#### Trapping Atoms with a $\text{CO}_2$ Laser

Another way to trap atoms in optical fields is the QUasi-ElectroStatic Trap (QUEST), where the light of a  $\text{CO}_2$  laser is used. Although the light of a  $\text{CO}_2$  laser at  $\lambda = 10.6 \mu\text{m}$  is far detuned from the atomic resonance in many atoms, the lasers are very powerful ( $P \approx 10 \text{ W}$ ) and can be focused down to small spotsizes ( $w \approx 50 \mu\text{m}$ ), which yields a very high intensity. This provides a trap depth of the order of  $100 \mu\text{K}$ . Since the light is detuned so far from resonance, the scattering rate of photons is negligible.

The QUEST trap has been studied extensively and the results are reviewed by Grimm et al. [61]. Recently, Barrett et al. [62] succeeded in using the QUEST trap to obtain quantum degeneracy. They loaded about  $30 \times 10^6$  atoms in an MOT and cooled the atoms by sub-Doppler cooling before being loaded in the QUEST trap. In the trap the initial phase-space density  $\rho$  is  $1/200$ , which is much higher than the usual. It then takes about  $2 \text{ s}$  to ramp down the power of the lasers and evaporatively cool the atoms over the BEC transition point, as shown in Figure 1.37. The number of condensed atoms is about  $3.5 \times 10^4$ . Recently, the group of Grimm in Innsbruck has succeeded in obtaining in a QUEST trap BEC for Cs. BEC for Cs has been searched for by many groups, but due to the special collision properties of the element at low energies large inelastic collision losses in magnetic traps have excluded evaporative cooling to the BEC transition point. In the QUEST atoms



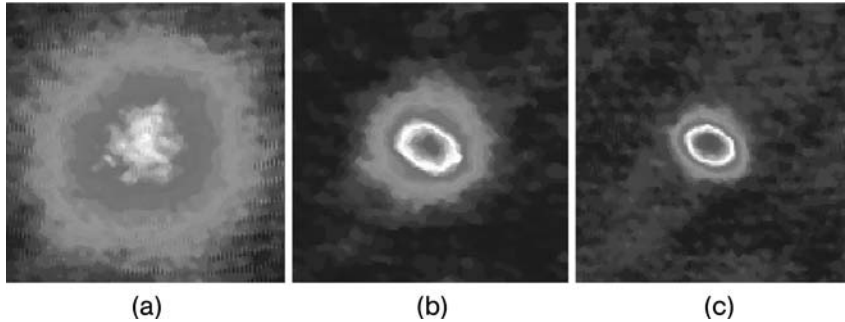


**Figure 1.37** Absorption images of (a) atoms above the BEC transition point ( $P = 480$  mW), (b) atoms below the transition point ( $P = 260$  mW), and (c) atoms in a pure condensate ( $P = 190$  mW). Here  $P$  denotes the power of the  $\text{CO}_2$  laser beam at the end of the evaporation cycle [62].

can be trapped in the lowest hyperfine state, where two-body inelastic losses are inhibited.

### 1.11

#### Conclusions

In this chapter, we have described the laser cooling and trapping techniques that have been used to cool and trap alkali-metal atoms for the attainment of BEC. We have emphasized the principles of the techniques used and described the most salient experimental results. Laser cooling and trapping is not only used to Bose condense atoms, but also is used in many experiments as a primary tool to obtain atoms with sufficient density and low temperatures to observe novel phenomena that cannot be studied otherwise. Based on the many experimental groups that work in this area, and the awarding of the Nobel prize twice in this field in the last 5 years, the field is very active and promises to deliver many new results in the years to come.

#### References

- 1 D. Wineland and H. Dehmelt. Proposed  $10^{14}\delta\nu/\nu$  Laser Fluorescence Spectroscopy on  $\text{Tl}^+$  Mono-Ion Oscillator. *Bull. Am. Phys. Soc.* **20**, 637 (1975).
- 2 T. Hansch and A. Schawlow. Cooling of Gases by Laser Radiation. *Opt. Commun.* **13**, 68–71 (1975).
- 3 H.J. Metcalf and P. van der Straten. *Laser Cooling and Trapping*. Springer, New York, 1999.
- 4 M.H. Anderson, J.R. Ensher, M.R. Matthews, C.E. Wieman, and E.A. Cornell. Observation of Bose–Einstein Condensation in a Dilute Atomic Vapor. *Science* **269**, 198–201 (1995).

- 5 C.C. Bradley, C.A. Sackett, J.J. Tollett, and R.G. Hulet. Evidence of Bose–Einstein Condensation in an Atomic Gas with Attractive Interactions. *Phys. Rev. Lett.* **75**, 1687–1690 (1995).
- 6 K. Davis, M-O. Mewes, M. Andrews, M. van Druten, D. Durfee, D. Kurn, and W. Ketterle. Bose–Einstein Condensation in a Gas of Sodium Atoms. *Phys. Rev. Lett.* **75**, 3969 (1995).
- 7 K. Huang. *Statistical Mechanics*. Wiley, New York, 1963.
- 8 L.D. Landau and E.M. Lifshitz. *Quantum Mechanics (Non-Relativistic Theory)*. Pergamon Press, Oxford, 1958.
- 9 E. Merzbacher. *Quantum Mechanics*. Wiley, New York, 1961.
- 10 L.I. Schiff. *Quantum Mechanics*. McGraw-Hill, New York, 1968.
- 11 M. Sargent III, M.O. Scully, and Jr. W.E. Lamb. *Laser Physics*. Addison-Wesley, Reading, 1974.
- 12 C. Cohen-Tannoudji, B. Diu, and F. Laloë. *Quantum Mechanics*. Wiley, New York, 1977.
- 13 B.H. Bransden and C.J. Joachain. *Physics of Atoms and Molecules*. Wiley, New York, 1983.
- 14 S. Stenholm. *Foundations of Laser Spectroscopy*. Wiley, New York, 1984.
- 15 B.H. Bransden and C.J. Joachain. *Introduction to Quantum Mechanics*. Longman, New York, 1989.
- 16 D.J. Griffiths. *Introduction to Quantum Mechanics*. Prentice-Hall, New Jersey, 1995.
- 17 P. Meystre and S. Stenholm (Eds.). The Mechanical Effects of Light. *J. Opt. Soc. Am. B* **2**, 1705–1872 (1985).
- 18 S. Chu and C. Wieman (Eds.). Laser Cooling and Trapping of Atoms. *J. Opt. Soc. Am. B* **6**, 1961–2288 (1989).
- 19 V. Minogin and V. Letokhov. *Laser Light Pressure on Atoms*. Gordon and Breach, New York, 1987.
- 20 H. Metcalf and P. van der Straten. Cooling and Trapping of Neutral Atoms. *Phys. Rep.* **244**, 204–286 (1994).
- 21 C.S. Adams and E. Riis. Laser Cooling and Trapping of Neutral Atoms. *Prog. Quant. Elect.* **21**, 1–79 (1997).
- 22 D. Wineland and W. Itano. Laser Cooling of Atoms. *Phys. Rev. A* **20**, 1521–1540 (1979).
- 23 W. Phillips and H. Metcalf. Laser Deceleration of an Atomic Beam. *Phys. Rev. Lett.* **48**, 596 (1982).
- 24 J. Prodan, W. Phillips, and H. Metcalf. Laser Production of a Very Slow Monoenergetic Atomic Beam. *Phys. Rev. Lett.* **49**, 1149 (1982).
- 25 V. Bagnato, G. Lafyatis, A. Martin, E. Raab, R. Ahmad-Bitar, and D. Pritchard. Continuous Stopping and Trapping of Neutral Atoms. *Phys. Rev. Lett.* **58**, 2194 (1987).
- 26 T.E. Barrett, S.W. Dapore-Schwartz, M.D. Ray, and G.P. Lafyatis. Slowing Atoms with ( $\sigma^-$ )-Polarized Light. *Phys. Rev. Lett.* **67**, 3483–3487 (1991).
- 27 R.J. Napolitano, S.C. Zilio, and V.S. Bagnato. Adiabatic Following Conditions for the Deceleration of Atoms with the Zeeman Tuning Technique. *Opt. Commun.* **80**, 110–114 (1990).
- 28 P.A. Molenaar, P. van der Straten, H.G.M. Heideman, and H. Metcalf. Diagnostic-Technique for Zeeman-Compensated Atomic-Beam Slowing – Technique and Results. *Phys. Rev. A* **55**, 605–614 (1997).
- 29 J. Dalibard and W. Phillips. Stability and Damping of Radiation Pressure Traps. *Bull. Am. Phys. Soc.* **30**, 748 (1985).
- 30 S. Chu, L. Hollberg, J. Bjorkholm, A. Cable, and A. Ashkin. Three-Dimensional Viscous Confinement and Cooling of Atoms by Resonance Radiation Pressure. *Phys. Rev. Lett.* **55**, 48 (1985).
- 31 P.D. Lett, R.N. Watts, C.E. Tanner, S.L. Rolston, W.D. Phillips, and C.I. Westbrook. Optical Molasses. *J. Opt. Soc. Am. B* **6**, 2084–2107 (1989).
- 32 D. Sesko, C. Fan, and C. Wieman. Production of a Cold Atomic Vapor Using Diode-Laser Cooling. *J. Opt. Soc. Am. B* **5**, 1225 (1988).
- 33 P. Gould, P. Lett, and W.D. Phillips. New Measurement with Optical Molasses. In W. Persson

- and S. Svanberg, editors, *Laser Spectroscopy VIII*, p. 64, Springer, Berlin, 1987.
- 34 T. Hodapp, C. Gerz, C. Westbrook, C. Furtlehner, and W. Phillips. Diffusion in Optical Molasses. *Bull. Am. Phys. Soc.* **37**, 1139 (1992).
  - 35 C. Cohen-Tannoudji and W.D. Phillips. New Mechanisms for Laser Cooling. *Phys. Today* **43**, 10, 33–40 (1990).
  - 36 P. Lett, R. Watts, C. Westbrook, W. Phillips, P. Gould, and H. Metcalf. Observation of Atoms Laser Cooled below the Doppler Limit. *Phys. Rev. Lett.* **61**, 169 (1988).
  - 37 E. Raab, M. Prentiss, A. Cable, S. Chu, and D. Pritchard. Trapping of Neutral-Sodium Atoms with Radiation Pressure. *Phys. Rev. Lett.* **59**, 2631 (1987).
  - 38 H. Metcalf. Magneto-Optical Trapping and Its Application to Helium Metastables. *J. Opt. Soc. Am. B* **6**, 2206–2210 (1989).
  - 39 J. Dalibard and C. Cohen-Tannoudji. Laser Cooling Below the Doppler Limit by Polarization Gradients – Simple Theoretical-Models. *J. Opt. Soc. Am. B* **6**, 2023–2045 (1989).
  - 40 P.J. Ungar, D.S. Weiss, S. Chu, and E. Riis. Optical Molasses and Multilevel Atoms – Theory. *J. Opt. Soc. Am. B* **6**, 2058–2071 (1989).
  - 41 B. Sheehy, S.Q. Shang, P. van der Straten, S. Hatamian, and H. Metcalf. Magnetic-Field-Induced Laser Cooling Below the Doppler Limit. *Phys. Rev. Lett.* **64**, 858–861 (1990).
  - 42 J. Dalibard. New Schemes in Laser Cooling. In S. Haroche, J.-C. Gay, and G. Grynberg, editors, *Atomic Physics XI*, p. 199, World Scientific, Singapore, 1989.
  - 43 S.Q. Shang, B. Sheehy, P. van der Straten, and H. Metcalf. Sub-Doppler Laser Cooling in a Magnetic Field. In R. Lewis and J. Zorn, editors, *Atomic Physics XII*, pp. 105–115, World Scientific, Singapore, 1991.
  - 44 C. Salomon, J. Dalibard, W.D. Phillips, A. Clairon, and S. Guellati. Laser Cooling of Cesium Atoms Below 3  $\mu$ K. *Europhys. Lett.* **12**, 683–688 (1990).
  - 45 W. Wing. On Neutral Particle Trapping in Quasistatic Electromagnetic Fields. *Prog. Quant. Elect.* **8**, 181 (1984).
  - 46 T. Bergeman, G. Erez, and H. Metcalf. Magnetostatic Trapping Fields for Neutral Atoms. *Phys. Rev. A* **35**, 1535 (1987).
  - 47 M.O. Mewes, M.R. Andrews, N.J. Vandrueten, D.M. Kurn, D.S. Durfee, and W. Ketterle. Bose–Einstein Condensation in a Tightly Confining DC Magnetic Trap. *Phys. Rev. Lett.* **77**, 416–419 (1996).
  - 48 T. Esslinger, I. Bloch, and T. W. Hänsch. Bose–Einstein condensation in a quadrupole-Ioffe-configuration trap. *Phys. Rev. A* **58**, R2664 (1998).
  - 49 N. Masuhara, J.M. Doyle, J.C. Sandberg, D. Kleppner, T.J. Greytak, H.F. Hess, and G.P. Kochanski. Evaporative Cooling of Spin-Polarized Atomic Hydrogen. *Phys. Rev. Lett.* **61**, 935 (1988).
  - 50 H.F. Hess. Evaporative Cooling of Magnetically Trapped and Compressed Spin-Polarized Hydrogen. *Phys. Rev. B* **34**, 3476 (1986).
  - 51 J.M. Doyle, J.C. Sandberg, I.A. Yu, C.L. Cesar, D. Kleppner, and T.J. Greytak. Hydrogen in the SubmilliKelvin Regime: Sticking Probability on Superfluid  $^4\text{He}$ . *Phys. Rev. Lett.* **67**, 603 (1991).
  - 52 O.J. Luiten, H.G.C. Werij, I.D. Setija, M.W. Reynolds, T.W. Hijmans, and J.T.M. Walraven. Lyman-Alpha Spectroscopy of Magnetically Trapped Atomic-Hydrogen. *Phys. Rev. Lett.* **70**, 544–547 (1993).
  - 53 I.D. Setija, H.G.C. Werij, O.J. Luiten, M.W. Reynolds, T.W. Hijmans, and J.T.M. Walraven. Optical Cooling of Atomic-Hydrogen in a Magnetic Trap. *Phys. Rev. Lett.* **70**, 2257–2260 (1993).
  - 54 K.B. Davis, M.O. Mewes, and W. Ketterle. An Analytical Model for Evaporative Cooling of Atoms. *App. Phys. B* **60**, 155–159 (1995).

- 55 W. Ketterle and N.J. van Druten. Evaporative Cooling of Trapped Atoms. *Adv. Atom. Mol. Opt. Phys.* **37**, 181 (1996).
- 56 V. Bagnato, D.E. Pritchard, and D. Kleppner. Bose–Einstein Condensation in an External Potential. *Phys. Rev. A* **35**, 4354 (1987).
- 57 S.E. Hamann, D.L. Haycock, G. Klose, P.H. Pax, I.H. Deutsch, and P.S. Jessen. Resolved-Sideband Raman Cooling to the Ground State of an Optical Lattice. *Phys. Rev. Lett.* **80**, 4149 (1998).
- 58 Andrew J. Kerman, Vladan Vuletic, Cheng Chin, and Steven Chu. Beyond Optical Molasses: 3D Raman Sideband Cooling of Atomic Cesium to High Phase-Space Density. *Phys. Rev. A* **84**, 439 (2000).
- 59 Steffen Wolf, Steven J. Oliver, and David S. Weiss. Suppression of Recoil Heating by an Optical Lattice. *Phys. Rev. Lett.* **85**, 4249 (2000).
- 60 Dian-Jiun Han, Steffen Wolf, Steven Oliver, Colin McCormick, Marshall T. DePue, and David S. Weiss. 3D Raman Sideband Cooling of Cesium Atoms at High Density. *Phys. Rev. Lett.* **85**, 724 (2000).
- 61 R. Grimm, M. Weidemüller, and Y. B. Ovchinnikov. Optical Dipole Traps for Neutral Atoms. *Adv. Atom. Mol. Opt. Phys.* **42**, 95 (2000).
- 62 M.D. Barrett, J.A. Sauer, and M.S. Chapman. All-Optical Formation of an Atomic Bose–Einstein Condensate. *Phys. Rev. Lett.* **87**, 010404 (2001).

## Appendix

### A Cooling Limits

In the tables in this appendix, characteristic values are given for the most important elements, which are laser cooled and trapped. In the case of metastable helium, two values are given, since there are two optical transitions, which can be used for laser cooling and trapping.

**Table A.1** Spectroscopic data for optical transitions that are used for laser cooling.<sup>a</sup>

	H	He*	He*	Li	Ne*	Na
<b>Mass <math>M</math></b>	<b>1</b>	<b>4</b>	<b>4</b>	<b>7</b>	<b>20</b>	<b>23</b>
Wavelength $\lambda$ (nm)	121.57	1083.0	388.86	670.08	640.2	589.0
Lifetime $\tau$ (ns)	1.6	97.85	98.38	27.3	19.42	16.1
Decay rate $\gamma$ ( $10^6/s$ )	625.0	10.2	10.2	36.6	51.5	62.1
Force $F_{\max}$ ( $10^{-21}$ N)	1703.0	3.12	8.7	18.1	26.6	34.9
Acceleration $a_{\max}$ $10^6$ m/s <sup>2</sup>	1017.0	0.47	1.30	1.55	0.80	0.94
	Ar*	K	Kr*	Rb	Xe*	Cs
<b>Mass <math>M</math></b>	<b>40</b>	<b>39</b>	<b>84</b>	<b>85</b>	<b>132</b>	<b>133</b>
Wavelength $\lambda$ (nm)	811.5	766.49	811.3	780.0	881.9	852.0
Lifetime $\tau$ (ns)	27.3	27.3	28.6	26.5	33.0	30.6
Decay rate $\gamma$ ( $10^6/s$ )	36.6	36.6	34.9	37.7	30.3	32.7
Force $F_{\max}$ ( $10^{-21}$ N)	14.9	15.8	14.3	16.0	11.4	12.7
Acceleration $a_{\max}$ $10^6$ m/s <sup>2</sup>	0.22	0.24	0.10	0.11	0.052	0.058

<sup>a</sup>From the spectroscopic data the maximum force and acceleration of the atoms can be calculated.

**Table A.2** Characteristic values for the excitation of the elements with laser light.<sup>a</sup>

	H	He*	He*	Li	Ne*	Na
Transition energy $\hbar\omega_0$ (eV)	10.199	1.144	3.188	1.850	1.937	2.105
wavenumber $k$ ( $10^6/m$ )	51.684	5.802	16.158	9.377	9.814	10.667
Decay rate $\gamma$ ( $10^6/s$ )	625	10.2	10.2	36.6	51.4	62.1
Cross section $\sigma_{ge}$ ( $10^{-15}/m$ )	7.1	560.0	72.2	214.4	195.7	165.6
Saturation intensity $I_s$ (W/m <sup>2</sup> )	72362	1.67	35.96	25.33	40.82	63.23

*continued overleaf*

Table A.2 Continued.

	Ar*	K	Kr*	Rb	Xe*	Cs
Transition energy $\hbar\omega_0$ (eV)	1.528	1.618	1.528	1.590	1.406	1.455
Wavenumber $k$ ( $10^6/\text{m}$ )	7.743	8.197	7.745	8.055	7.125	7.374
Decay rate $\gamma$ ( $10^6/\text{s}$ )	36.6	36.6	35.0	37.7	30.3	32.7
Cross section $\sigma_{\text{ge}}$ ( $10^{-15} \text{ m}^2$ )	314.4	280.5	314.3	290.5	371.3	346.6
Saturation intensity $I_s$ ( $\text{W}/\text{m}^2$ )	14.26	16.92	13.62	16.54	9.19	10.99

<sup>a</sup>The cross section and saturation intensity are valid for the strongest transition.

Table A.3 Cooling limits for the velocity and temperature of laser cooling for different elements.<sup>a</sup>

	H	He*	He*	Li	Ne*	Na
Capture limit:						
Velocity $v_{\text{in}}$ (m/s)	12.09	1.76	0.63	3.91	5.25	5.82
temperature $T_{\text{in}}$ (mK)	17.7	1.49	0.19	12.9	66.2	93.8
Doppler limit:						
velocity $v_{\text{D}}$ (m/s)	4.44	0.28	0.28	0.41	0.29	0.29
temperature $T_{\text{D}}$ ( $\mu\text{K}$ )	2386	39.0	38.8	139.9	196.7	237.2
Recoil limit:						
velocity $v_{\text{r}}$ (m/s)	3.25	0.092	0.26	0.085	0.031	0.029
temperature $T_{\text{r}}$ ( $\mu\text{K}$ )	1285	4.08	31.6	6.07	2.34	2.40
	Ar*	K	Kr*	Rb	Xe*	Cs
Capture limit:						
velocity $v_{\text{in}}$ (m/s)	4.73	4.47	4.51	4.68	4.25	4.43
temperature $T_{\text{in}}$ (mK)	107.6	93.6	205.8	224.2	287.1	314.0
Doppler limit:						
velocity $v_{\text{D}}$ (m/s)	0.17	0.17	0.11	0.12	0.085	0.088
temperature $T_{\text{D}}$ ( $\mu\text{K}$ )	139.9	139.9	133.5	144.1	115.7	124.8
Recoil limit:						
velocity $v_{\text{r}}$ (m/s)	0.012	0.013	0.006	0.006	0.0034	0.0035
temperature $T_{\text{r}}$ ( $\mu\text{K}$ )	0.73	0.84	0.35	0.37	0.19	0.20

<sup>a</sup>The capture limit is characteristic for the range of velocities that can be captured in optical molasses. The Doppler limit is the limit for cooling on a two-level atom. The recoil limit is the limit for laser cooling using sub-Doppler processes.